# ON THE TRANSONIC AERODYNAMICS OF A COMPRESSOR BLADE ROW

By J.C. Erickson, Jr., J.A. Lordi, W.J. Rae

CAL NO. AI-3003-A-1

Prepared For:

National Aeronautics and Space Administration
Research Division
Office of Advanced Research and Technology
Code RRF
Washington, D.C. 20546

FINAL REPORT
NASW-2091
OCTOBER 1971

CORNELL AERONAUTICAL LABORATORY, INC.
Buffalo, New York 14221

# ON THE TRANSONIC AERODYNAMICS OF A COMPRESSOR BLADE ROW

Final Report
CAL Report No. AI-3003-A-1
Contract No. NASW-2091
October 1971

Prepared for:

Headquarters
National Aeronautics and Space Administration
Research Division
Office of Advanced Research and Technology
Code RRF
Washington, D. C. 20546

Prepared by: J. C. Erickson, Jr.
J. A. Lordi
W. J. Rae

Approved by: for C. E. Treanor
Head, Aerodynamic
Research Department

# FOREWORD

This report documents the investigation performed under Contract NASW-2091 during the period from August 1970 to September 1971. The investigation was administered for NASA Headquarters by Mr. I. R. Schwartz, Dr. W. H. Roudebush and Mr. A. Gessow.

The authors wish to thank Mr. J. J. Kramer, Chief of the Propulsion System Acoustics Branch of the NASA Lewis Research Center, and members of his branch for their contributions during several technical discussions. The authors also wish to thank Mr. J. R. Moselle of CAL for his efficient programming of the analysis for machine computation.

## SUMMARY

Linearized analyses have been carried out for the induced velocity and pressure fields within a blade row operating in an infinite annulus at transonic Mach numbers of the flow relative to the blades. In addition, the relationship between the induced velocity and the shape of the mean blade surface has been determined. A computational scheme has been developed for evaluating the blade mean surface ordinates and surface pressure distributions. The separation of the effects of a specified blade thickness distribution from the effects of a specified distribution of the blade lift has been established. In this way, blade mean surface shapes that are necessary for the blades to be locally nonlifting have been computed and are presented for two examples of blades with biconvex parabolic arc sections of radially tapering thickness. Blade shapes that are required to achieve a zero thickness, uniform chordwise loading, constant work spanwise loading are also presented for two examples. In addition, corresponding surface pressure distributions are given. The flow relative to the blade tips has a high subsonic Mach number in the examples that have been computed. The results suggest that at near-sonic relative tip speeds the effective blade shape is dominated by the thickness distribution, with the lift distribution playing only a minor role.

TABLE OF CONTENTS

## LIST OF SYMBOLS

| | |
|---|---|
| $a$ | Chordwise loading parameter |
| $a_\infty$ | Undisturbed speed of sound |
| $A_{nk}$ | Coefficient in elementary solution, Eq (2) |
| $B$ | Number of blades |
| $c$ | Chord length |
| $c_a$ | $c \cos\psi$, axial projection of blade chord |
| $C_p$ | Pressure coefficient, Eq (17) |
| $\hat{C}_p$ | Part of $C_p$ that is symmetrical above and below the blade mean surface in the lifting case |
| $f$ | Normalized radial thickness distribution |
| $F$ | Source strength |
| $g_1$ | Blade thickness shape function, given in Eq (22) for biconvex parabolic arc sections |
| $g_2$ | Blade loading shape function, given in Eq (51) for uniform chordwise loading |
| $G_{mk}$ | Mode amplitude factors for loading case, Eqs (42) to (45) |
| $h$ | Ratio of hub radius to tip radius |
| $H_{mk}$ | Fourier-Bessel expansion coefficient for wake functions in lifting case |
| $i$ | $\sqrt{-1}$ |
| $I_n$ | Modified Bessel function of the first kind |
| $J_n$ | Bessel function of the first kind |
| $k$ | Radial mode number |
| $K_{nk}$ | Radial eigenvalues, roots of Eq (6) |
| $K_n$ | Modified Bessel function of the second kind |
| $L_{mk}$ | Function of $\rho$ introduced in Eqs (52) and (53), given in Eq (54) |
| $L_T$ | Blade spacing at the tips |
| $m$ | Circumferential mode number |
| $M$ | $U/a_\infty$ , axial Mach number |
| $M_T$ | $\omega r_T/a_\infty$, blade tip speed divided by undisturbed sound speed |
| $M_R$ | $(M^2+M_T^2)^{1/2}$, relative Mach number at blade tips |
| $n$ | Coordinate normal to $r$ and $s$ , Fig. 2 |
| $\eta$ | Mean blade surface ordinate, Fig. 2 |

$N^c_{m\ell}, N^s_{m\ell}$ Functions of $\bar{z}$ introduced in Eq (24) for the thickness case and in Eq (53) for the lifting case, given in Table I for biconvex parabolic arc sections and in Table II for uniform chordwise loading

$N_{n\ell}$ Normalization constant in Eq (5)

$p$ Static pressure perturbation, Eq (11)

$p_o$ Total pressure in duct-fixed coordinates

$Q_{mB\ell}$ Fourier-Bessel expansion coefficient for source strength, Eq (10)

$Q^*_{mB\ell}$ Form of $Q_{mB\ell}$ for radially similar thickness profiles, Eq (21)

$r$ Radial coordinate, Fig. 1

$R_n$ Normalized combination of Bessel functions of the first and second kinds, Eq (5)

$R_\infty$ Total pressure ratio between points far upstream and downstream, Eq (46)

$s$ Coordinate along the helix of advance and normal to $n$ and $r$, Fig. 2

$S^c_{m\ell}, S^s_{m\ell}$ Functions of $\bar{z}$ introduced in Eq (23) for the thickness case and in Eq (52) for the lifting case, given in Table I for biconvex parabolic arc sections and in Table II for uniform chordwise loading

$t$ Time

$T_{m\ell}$ Function of $\rho$ introduced in Eqs (23) and (24), given in Eq (25)

$u$ Perturbation in axial velocity

$u_n$ Component of perturbation velocity in $n$-direction

$u_s$ Component of perturbation velocity in $s$-direction

$U$ Undisturbed axial velocity, Figs. 1 and 2

$U_o$ $U/\cos\psi$, resultant velocity incident to blade section, Fig. 2

$v_\theta$ Perturbation in tangential velocity

$x$ Axial coordinate, Fig. 1

$Y_n$ Bessel function of the second kind

$\bar{z}$ $\omega x/U$, dimensionless axial coordinate

$Z$ Bessel function cross product, Eq (32)

$\beta$ $\sqrt{1 - M^2}$

$\gamma$ Bound vortex strength

$\bar{\gamma}$ Ratio of specific heats

$\gamma_{n\ell}$ Phase factor in definition of $R_n$, Eq (5)

$\Gamma$ Bound circulation strength

$\bar{\Gamma}$ Radial average of $\Gamma$, Eq (33)

$\Gamma_{m\ell}$ Fourier-Bessel expansion coefficient for bound circulation

$\delta_x$ $\omega c_a / U$ , dimensionless axial projection of blade chord

$\zeta$ $\theta - z$ , helical coordinate

$\zeta_\ell$ $\zeta - \frac{(2\ell+1)\pi}{B}$, $\ell = 0, 1, \ldots, (B-1)$, function varying linearly from $-\pi/B$ to $\pi/B$ between adjacent blades

$\theta$ Angular coordinate, Fig. 1

$\lambda_{n\ell}$ Axial eigenvalue, Eq (3)

$\xi$ Axial projection of distance along blade surface

$\rho$ $\omega r/U$, dimensionless radial coordinate

$\rho_\infty$ Undisturbed density

$\sigma_\infty$ $R_\infty - 1$, normalized total pressure rise factor

$\tau$ Thickness-to-chord ratio

$\tau_o$ Value of $\tau$ at hub

$\varphi$ Velocity potential

$\varphi_{n\ell}$ Elementary solution of Eq (1) for velocity potential, Eq (2)

$\varphi_w$ Wake velocity potential, Eq (30)

$\chi_m$ Wake function, Eq (31)

$\psi$ $\cos^{-1}\left[(1+\rho^2)^{-1/2}\right]$ , angle between $U$ and $U_o$ at a radial station, Fig. 2

$\omega$ Angular velocity of blade row, Fig. 1

Subscripts:

1 Fluid fixed coordinates

$\infty$ Undisturbed quantities

H Hub value

T Tip value

Superscripts:

$d$ Downstream of blade row

$i$ Within blade row

$u$ Upstream of blade row

$( )'$ Derivative of quantity with respect to its argument

# I. INTRODUCTION

The transonic flow through an axial compressor exhibits many extremely complicated phenomena. No single analysis can account adequately for three-dimensional effects, the presence of shock waves and end-wall boundary layers, interference among blade rows, finite duct effects and other features of the flow. In the present report attention is focused on the three-dimensional effects in the flow field of a single blade row rotating in an infinite duct. Examination of the three-dimensional effects provides an understanding of some important aspects of the flow over the blades for both compressor performance and noise generation.

A linearized theory for this flow has been developed by McCune (Refs 1 and 2) with more recent extensions by Okurounmu and McCune (Refs 3 and 4). Their basic solutions for the flow through such a blade row are appropriate not only for computing the flow field in the immediate vicinity of the blades but also for computing the flow field far up- and downstream of the blade row.

The acoustic far field of the rotating blade row has been examined within the context of this theory at Cornell Aeronautical Laboratory, Inc. in a related study and has been reported in Refs 5 and 6. The importance of that research effort is that the acoustic field can be related directly to the geometry of the blades and the aerodynamics of the flow through the blade row. Many previous workers (see Refs 7 to 10, for example) have examined the acoustic field in such an infinite duct, but with the approximation that the blade forces were assumed to be known.

In the present investigation, the flow field characteristics within the blade row, and in particular at the blades themselves, have been examined. In Refs 5 and 6, the noise generation has been separated, in the linearized sense, into noise due to blade thickness and noise due to blade lift. The blade thickness distribution is assumed to be known in the thickness case and the pressure difference across the blade surface is assumed to be known in the lifting case. These are sufficient to compute the acoustic far field. In this

study, then, the relationship between the blade geometry and the specified blade thickness and pressure differences is completed by determining the ordinates of the mean blade surfaces and the portion of the pressure distributions which are symmetrical above and below the mean surfaces.

The separation of the flow field into thickness and lifting parts is discussed in Section II. The concept of a mean blade surface shape that is induced solely by blade thickness through three-dimensional interactions is of special importance and is covered in that section. In Section III, the flow field within the blade row is examined for thickness alone, with numerical results presented in two cases for the blade mean surface shapes and the blade surface pressures. The flow field within the blade row and similar numerical results are examined for lifting blades in Section IV. Finally, concluding remarks are given in Section V.

## II. SEPARATION OF THICKNESS AND LIFTING CASES

The complete independence of the wing thickness and lifting effects in the linearized representation of a two- or three-dimensional planar wing is well established, see Refs 11 and 12, for example. The wing may be considered to have a mean surface shape, above and below which the thickness is distributed symmetrically. The thickness is represented mathematically by a surface distribution of sources along a planar surface approximating the wing, while the pressure difference across the wing is represented by a surface distribution of either doublets or, as used here, vortices along the same planar surface.

A planar source distribution has the property that each elemental source induces a discontinuity in normal velocity across the surface locally, but does not induce a normal velocity component anywhere else along the surface. In addition, each elemental source induces a tangential velocity component everywhere along the surface. This tangential velocity component is continuous across the planar surface and is directly proportional to the surface pressure. If the thickness distribution is specified, then, the boundary condition that the wing upper and lower surfaces be streamlines leads directly to a relationship between the chordwise derivative of the thickness distribution and the source strength. The tangential velocity, and so the surface pressure, can then be found directly by integration over the source distribution. If, on the other hand, the tangential velocity or pressure is specified, a singular integral equation must be solved to determine the source strength. When the solution for the source strength has been found, the resulting thickness distribution follows directly from the streamline boundary condition by integration.

A planar vortex distribution has the property that each elemental vortex induces a discontinuity in the tangential velocity, and so in the surface pressure, across the surface locally, but does not induce a tangential velocity component anywhere else along the surface. In addition, each elemental vortex induces a normal velocity component everywhere along the surface. This normal component is continuous across the planar surface. If the

distribution of the tangential velocity difference, or equivalently the pressure difference, across the surface is specified, then, the vortex distribution can be determined directly in terms of the local tangential velocity difference. The boundary condition that the wing mean surface be a streamline leads directly to the chordwise derivative of the mean surface shape by an integration over the vortex distribution. The mean surface ordinates are found by integration. If, on the other hand, the mean surface ordinates, and so the chordwise derivatives, are specified, the streamline boundary condition becomes a singular integral equation for the vortex distribution. When the solution for the vortex distribution has been found, the tangential velocity difference, pressure difference and the lift follow directly.

Once the wing is no longer planar, for example if dihedral or twist of the wing is present or if a lifting system composed of several wings is considered, the separation of thickness and lift is not so straightforward. The elemental sources, although still inducing only a normal velocity jump locally, do induce a normal velocity component along the mean surface at points that do not lie in the same plane. This normal velocity is continuous across the mean surface. In a similar way, the elemental vortices, although still inducing only a tangential velocity jump locally, do induce a tangential velocity component along the mean surface at points that do not lie in the same plane. This tangential velocity is also continuous across the mean surface. These additional normal and tangential induced velocity components lead generally to a coupling between the thickness and lifting effects that is not present for a planar wing.

The acoustic intensity has been determined separately for blade thickness and blade lift in Refs 5 and 6. In this way each effect may be assessed separately. In the nonlifting case when thickness alone is treated, it is important to realize that the blades are assumed to be nonlifting locally, i.e., the pressure difference across the blades is everywhere zero. It is not sufficient to consider only the total integrated lift to be zero. The so-called design problem has been considered in Refs 5 and 6, i.e., it is assumed that in the thickness case the thickness distribution is known while in the lifting case the pressure difference across the blade surface is known. In this way, it is not

necessary to solve any integral equations, as discussed above. It may be noted that specification of the distributions of thickness and pressure difference are the standard procedure used in marine propeller design, see Ref 13, for example.

When thickness alone is considered for the three-dimensional geometry in which there are many interfering, highly twisted blades, it must be recognized that the source distributions on the blades give rise to a normal velocity component that is continuous across the mean blade surfaces. In order for the pressure difference across the blades to be zero everywhere, i. e., to be locally nonlifting, the mean blade surfaces must be shaped so that they are streamlines with respect to this induced normal velocity. That is, the inherent coupling between thickness and lift must be broken by shaping the mean blade surfaces so that the blades carry no lift anywhere on their surfaces. This procedure has been used in marine propeller design by Kerwin and Leopold (Refs 13 and 14) to determine a blade incidence correction due to thickness.

When lifting alone is considered for infinitely thin blades, it must be recognized that the vortex distributions on the blades give rise to a tangential velocity component that is continuous across the blade surfaces as well as a normal component. The normal component again leads to the shaping of the mean blade surfaces so that they are streamlines of the flow. However, the mean surface shapes in the lifting case are those necessary to provide the specified pressure difference across the blades. The tangential component due to lift leads to a pressure distribution on the blade surfaces that is symmetrical above and below the mean blade surface.

Only the design problem is considered in this report. However, the design problem can be extremely useful from both the acoustic and performance points of view since it can yield the mean blade surface shapes that are necessary to achieve desirable acoustical or performance properties. Moreover, successful treatment of the design problem is a requisite first step towards treatment of the problem in which the thickness and mean blade surface shapes are completely specified and the acoustic and performance characteristics must be determined. The coupling between thickness and loading is much more complex in this case because an integral equation must be solved.

## III. FLOW FIELD WITHIN BLADE ROW DUE TO BLADE THICKNESS

### 1. SUMMARY OF BASIC ANALYSIS

McCune's analysis (Ref 1) treats a rotating blade row in an infinite annulus. In fluid fixed coordinates, the blade row advances with axial velocity $U$ and rotates with angular velocity $\omega$ (see Fig. 1). If the blades are sufficiently thin so that only small disturbances are generated, the disturbance velocity potential satisfies the wave equation in fluid fixed coordinates. In a cylindrical system ( $r$ , $\theta$ , $x$ ) fixed to the blades, the flow becomes steady and the governing equation for velocity potential $\varphi$ becomes

$$\beta^2 \varphi_{zz} + \frac{1}{\rho^2}(1 - M^2\rho^2)\varphi_{\theta\theta} - 2M^2\varphi_{\theta z} + \varphi_{\rho\rho} + \frac{1}{\rho}\varphi_{\rho} = 0 \qquad (1)$$

where $z = \omega x/U$ , $\rho = \omega r/U$ , $M = U/a_\infty$ , $\beta^2 = 1 - M^2$

and $a_\infty$ is the undisturbed sound speed. The elementary solution to the above equation is

$$\varphi_{nk} = A_{nk} \exp\left\{in\theta + \left(\frac{inM^2}{\beta^2} \pm \lambda_{nk}\right)z\right\} R_n\left(K_{nk}\frac{\rho}{\rho_T}\right) \qquad (2)$$

where the plus sign holds for $z < 0$ and the minus sign for $z > 0$ , and

$$\lambda_{nk} = \frac{n}{\rho_T \beta^2}\sqrt{\beta^2\left(\frac{K_{nk}}{n}\right)^2 - M_T^2} \qquad (3)$$

$$M_T = \omega r_T / a_\infty \qquad (4)$$

where $r_T$ is the blade tip radius.

The elementary solution given in Eq (2) involves the circumferential eigenfunction $e^{in\theta}$ and the radial eigenfunction $R_n$ . For the case of $B$ radially oriented line sources rotating in an infinite annulus, $n = mB$ where $m$

is the circumferential mode number and $R_{mB}$ is a normalized combination of the Bessel functions of the first and second kind of order $mB$, namely

$$R_{mB}\left(K_{mBk}\frac{\rho}{\rho_T}\right) = \frac{1}{N_{mBk}}\left[J_{mB}\left(K_{mBk}\frac{\rho}{\rho_T}\right) - \frac{\gamma_{mBk}}{\sqrt{3}}\,Y_{mB}\left(K_{mBk}\frac{\rho}{\rho_T}\right)\right] \quad (5)$$

The factor $N_{mBk}$ is a normalization factor; $K_{mBk}$ is the kth root of the equation

$$J'_{mB}(h\eta)\,Y'_{mB}(\eta) - J'_{mB}(\eta)\,Y'_{mB}(h\eta) = 0 \quad (6)$$

which results from the boundary condition that the radial velocity vanish at the inner and outer annulus radii; $h$ is the ratio of the hub radius to the tip radius; and $\gamma_{mBk}$ is a phase factor given by

$$\frac{\gamma_{mBk}}{\sqrt{3}} = \frac{J'_{mB}(K_{mBk})}{Y'_{mB}(K_{mBk})} = \frac{J'_{mB}(hK_{mBk})}{Y'_{mB}(hK_{mBk})} \quad (7)$$

From Eq (3) it can be seen that $\lambda_{mBk}$ changes from a real quantity to an imaginary one when the quantity $M_T = \omega r_T / a_\infty$ becomes greater than $\beta K_{mBk}/mB$. This is the cutoff phenomenon discussed by Tyler and Sofrin (Ref 7) for duct acoustic modes. When $\lambda_{mBk}$ is real, the $m$, $k$ mode is damped rapidly with distance away from the blade row. When $\lambda_{mBk}$ is imaginary, the mode propagates undamped along the duct as a so-called "spinning acoustic wave." For $U = 0$, i.e., no through flow, the cutoff condition reduces to $M_T = K_{mBk}/mB$, as obtained in Ref 7. For $m = 0$, $\lambda_{0k} = K_{0k}/\beta\rho_T$, which is always real, and hence this mode always decays. In the limit $mB \to \infty$ for fixed $k$, the radial eigenvalues become $K_{mBk}/mB \sim 1 + 0(mB)^{-2/3}$. If the first term of this limit is used, the cutoff condition is that the relative Mach number at the blade tips, $M_R = (M^2 + M_T^2)^{1/2}$, be supersonic.

McCune (Ref 1) distributed sources over the helical surfaces which represent the blades and expanded these source distributions in a Fourier-Bessel series of the elementary solutions. In this way, he obtained the following solution for the velocity potential, real part implied,

$$\varphi^{u,d} = -\frac{B}{4\pi\beta^2}\int_0^{[c_a(\rho)]_{max}} \sum_{m=-\infty}^{\infty}\sum_{k=1}^{\infty} \frac{Q_{mBk}(\xi)}{\lambda_{mBk}} R_{mB}\left(K_{mBk}\frac{\rho}{\rho_T}\right) \times \exp\left\{ imB\left(\theta - \frac{\omega\xi}{U}\right) + \left(\frac{imBM^2}{\beta^2} \pm \lambda_{mBk}\right)\left(z - \frac{\omega\xi}{U}\right)\right\} d\xi \tag{8}$$

$$\varphi^{i} = -\frac{B}{4\pi\beta^2}\int_0^{[c_a(\rho)]_{max}} \sum_{m=-\infty}^{\infty}\sum_{k=1}^{\infty} \frac{Q_{mBk}(\xi)}{\lambda_{mBk}} R_{mB}\left(K_{mBk}\frac{\rho}{\rho_T}\right) \times \exp\left\{ imB\left(\theta - \frac{\omega\xi}{U}\right) + \frac{imBM^2}{\beta^2}\left(z - \frac{\omega\xi}{U}\right) - \lambda_{mBk}\left|z - \frac{\omega\xi}{U}\right|\right\} d\xi \tag{9}$$

where $\xi$ is the axial projection of distance along the blade surface at a given radius and $c_a(\rho)$ is the projection of the blade chord $c(\rho)$ on the $x$ axis. The plus sign and the superscript $u$ refer to the region upstream of the point along the leading edge that lies farthest upstream, i.e. $z = 0$; the minus sign and $d$ refer to the region downstream of the point along the trailing edge that lies farthest downstream, i.e. $z = [c_a(\rho)]_{max}$; and the superscript $i$ refers to those points within the blade row itself, i.e. $0 < z < [c_a(\rho)]_{max}$. The quantities $Q_{mBk}(\xi)$, which are the coefficients in the expansion of the source strength, $F(\rho,\xi)/\rho$, are given by

$$Q_{mBk}(\xi) = \frac{1}{\rho_T}\int_h^1 F(\rho,\xi)\sqrt{1+\rho^2}\, R_{mB}\left(K_{mBk}\frac{\rho}{\rho_T}\right) d\left(\frac{\rho}{\rho_T}\right) \tag{10}$$

From this solution for the velocity potential, the perturbation pressure and velocities anywhere in the flow field can be calculated. In blade fixed coordinates the pressure and velocity perturbations are given by

$$u = \frac{\omega}{U}\frac{\partial\varphi}{\partial z}, \quad v_\theta = \frac{1}{r}\frac{\partial\varphi}{\partial\theta}, \quad p = -\rho_\infty(Uu + \omega r v_\theta) \tag{11}$$

where $\rho_\infty$ is the undisturbed density. It is more convenient for consideration

of the flow within the blade row to use a coordinate system aligned with the undisturbed helical flow incident to the blades. A typical blade section at some radius $r$ is shown in Fig. 2. The coordinate $s$ lies along the helix of advance, i.e. it is aligned with the local incident velocity $U_o$ which is the resultant of the axial free stream velocity $U$ and the local rotational component $\omega r$. The coordinate $n$ is normal to both $r$ and $s$ in a right-handed coordinate system ($r$, $n$, $s$) and is directly proportional, at a given radius, to the helical coordinate $\zeta = \theta - z$ that often occurs in the theory of rotating machinery. The velocity components in Eqs (11) can be resolved into components $u_s$ and $u_n$, say, in the $s$ and $n$ directions, respectively, namely

$$u_s = \frac{\omega}{U_o}\left(\frac{\partial \phi}{\partial z} + \frac{\partial \phi}{\partial \theta}\right) \tag{12}$$

$$u_n = \frac{\omega}{U_o \rho}\left(-\rho^2 \frac{\partial \phi}{\partial z} + \frac{\partial \phi}{\partial \theta}\right) \tag{13}$$

or

$$u_n = -\rho u_s + \frac{\omega(1+\rho^2)}{U_o \rho}\frac{\partial \phi}{\partial \theta} \tag{14}$$

where, from Fig. 2

$$U_o = U\sqrt{1+\rho^2} \tag{15}$$

The perturbation pressure, $p$, from Eqs (11) then reduces simply to

$$p = -\rho_\infty U_o u_s \tag{16}$$

or, in coefficient form,

$$C_p \equiv \frac{p}{\frac{1}{2}\rho_\infty U^2} = -\frac{2(1+\rho^2)u_s}{U_o} \tag{17}$$

The ordinates of the mean blade surface that is required for the blades to be locally nonlifting, $\eta(s)$ in Fig. 2, may be found from the boundary condition that the mean surface be a streamline. In the linearized approximation

this boundary condition yields the differential equation

$$\frac{d\eta(s)}{ds} = \frac{u_n(r, n=0, s)}{U_o} \tag{18}$$

Eq (18) is integrated with the condition that $\eta(\frac{c}{2}) = 0$ in order to compare blade ordinates.

The expressions for the velocity potential given in Eqs (8) and (9) are greatly simplified by assuming that the blade profiles are similar at each radial station and that the projection of the chord on the axis is a constant, $c_a$. For radially similar profiles, the source strength $F(\rho, \xi)/\rho$ is

$$F(\rho, \xi) = \tau(\rho)\, g_1(\xi) \tag{19}$$

where $\tau(\rho)$ is the thickness ratio at each radius and $g_1(\xi)$ describes the blade shape. Assuming $\tau(\rho)$ in the form $\tau(\rho) = \tau_o f(\rho)$ where $\tau_o$ is the thickness ratio at the hub and $f(\rho)$ is a function which is unity at the hub and describes the radial variation of the thickness ratio, then

$$Q_{mBk}(\xi) = \tau_o\, g_1(\xi)\, Q^*_{mBk} \tag{20}$$

where

$$Q^*_{mBk} = \frac{1}{\rho_T} \int_h^1 f(\rho) \sqrt{1+\rho^2}\, R_{mB}\left(K_{mBk} \frac{\rho}{\rho_T}\right) d\left(\frac{\rho}{\rho_T}\right) \tag{21}$$

In the case of biconvex parabolic arc sections, the integration of each term in the expression for the velocity potential may be done in closed form. For parabolic arcs

$$g_1(\xi) = 4U\left(1 - \frac{2\xi}{c_a}\right) \tag{22}$$

This form has been used for $g_1(\xi)$ throughout the present work. However, the $\xi$ integration can be done for any polynomial variation of $g_1(\xi)$.

The streamwise, $u_s$, and normal, $u_n$, components of the induced velocity anywhere within the blade row can be found for the biconvex parabolic arc thickness distribution by evaluating Eqs (12) and (14) by means of Eqs (9), (20), (21) and (22). In general form this gives

$$\frac{u_s}{U_o \tau_o} = -\frac{2B}{\pi\beta^2} \sum_{m=0}^{\infty} \sum_{k=1}^{\infty} T_{mk}(\rho) \left[ S^c_{mk}(z) \cos mB\zeta + S^s_{mk}(z) \sin mB\zeta \right] \quad (23)$$

$$\frac{u_n}{U_o \tau_o} = -\rho \left[ \frac{u_s}{U_o \tau_o} \right] + \frac{2B}{\pi\beta^2} \sum_{m=1}^{\infty} \sum_{k=1}^{\infty} \frac{mB(1+\rho^2)}{\rho} T_{mk}(\rho) \left[ N^c_{mk}(z) \cos mB\zeta + N^s_{mk}(z) \sin mB\zeta \right] \quad (24)$$

where

$$T_{mk}(\rho) = \frac{Q^*_{mBk} R_{mB}(K_{mBk}\, \rho/\rho_T)}{1+\rho^2}, \qquad m \geq 0 \quad (25)$$

The quantities $S^c_{mk}$, $S^s_{mk}$, $N^c_{mk}$ and $N^s_{mk}$ are functions of $z$ only, but have different forms depending upon the magnitude of the relative tip Mach number. For subsonic relative tip Mach numbers, all $\lambda_{mBk}$ in Eq (3) are real, while for supersonic relative tip Mach numbers, some or all of the $\lambda_{mBk}$ will be imaginary and so lead to different forms for $S^c_{mk}$, etc. because the real part of Eq (9) must be taken to obtain Eqs (23) and (24). In the present report attention is concentrated on subsonic relative tip speeds and the appropriate values of $S^c_{mk}$, etc. are given in Table I.

Evaluation of the blade mean surface pressure distribution and ordinates requires expressions for $u_s$ and $u_n$ on the linearized location of the mean surface, namely $n = 0$, or in terms of $\theta$ and $z$, for $\zeta = \theta - z = \frac{2j\pi}{B}$, $j = 0, 1, \ldots, (B-1)$. Equation (23) for $u_s$ may be evaluated easily in this limit since the summation over $S^s_{mk}(z) \sin mB\zeta$ vanishes and $u_s$ is continuous across the mean blade surface. The result is

$$\frac{u_s(r, n=0, s)}{U_o \tau_o} = -\frac{2B}{\pi\beta^2} \sum_{m=0}^{\infty} \sum_{k=1}^{\infty} T_{mk}(\rho)\, S^c_{mk}(z) \quad (26)$$

The normal component $u_n$, however, has a discontinuity across the mean

blade surface that is related directly to the source strength. Through an analysis of the first term in $N^{s}_{mk}$ in Table I it can be shown that summation of the series will lead to the discontinuity when approaching $\zeta = \frac{2j\pi}{B}$ from above and below the mean surface, with a value of zero at the surface. Therefore the continuous part of $u_n$ at the mean blade surface, which is the part required in Eq (18), is given by

$$\frac{u_n(r, n=0, s)}{U_o \tau_o} = -\rho\left[\frac{u_s(r, n=0, s)}{U_o \tau_o}\right] + \frac{2B}{\pi\beta^2}\sum_{m=1}^{\infty}\sum_{k=1}^{\infty}\frac{mB(1+\rho^2)}{\rho} T_{mk}(\rho) N^{c}_{mk}(z) \tag{27}$$

## 2. METHOD OF COMPUTATION

The principal task in evaluating $u_s$ and $u_n$ on the mean blade surface from Eqs (26) and (27) is the computation of $T_{mk}$. The $S^{c}_{mk}$ and $N^{c}_{mk}$ terms in Table I are complicated algebraically, but can be computed easily.

Computation of $T_{mk}$ involves evaluation of $K_{mBk}$ and $Q^{*}_{mBk}$. In the present application to fans and compressors, these computations require repeated calculations of the Bessel functions of the first and second kinds of large order. In performing the calculations, the asymptotic expansions derived by Olver (Ref 15) for the Bessel functions of large order, which are uniformly valid for all arguments, have been used and greatly facilitate the computations. The methods developed to apply Olver's expansions to the evaluation of $K_{mBk}$ and $Q^{*}_{mBk}$ are described in Appendix B of Ref 5. Fortunately $K_{mBk}$ and $\rho_T Q^{*}_{mBk}$ are functions only of the blade number $B$, the ratio of hub radius to the tip radius $h$, and the radial distribution of thickness $f(\rho)$, see Eqs (5) to (7) and (21). Thus $K_{mBk}$ and $\rho_T Q^{*}_{mBk}$ may be computed once and for all with fixed $B$, $h$ and $f(\rho)$. A computer program has been written to perform these operations.

A separate computer program has been written to evaluate $u_s/U_o\tau_o$, $u_n/U_o\tau_o$ and $C_p/\tau_o$. This program requires as input the values of $K_{mBk}$ and $\rho_T Q^{*}_{mBk}$ found from the first program as well as the compressor operating conditions. For the cases run to date and reported here, Eq (18)

was integrated by hand, but an integration subroutine developed subsequently for the lifting case can be used.

McCune did not compute $u_n$ in Refs 1 and 2, but he did evaluate the pressure coefficient $C_p/\tau_o$. This evaluation was carried out in an entirely different way from that described above, namely he computed the velocity potential along the mean blade surface and differentiated it numerically. The analysis of Refs 1 and 2 was completed prior to the development of Olver's expansions (Ref 15), so alternate methods were derived to evaluate $K_{mBk}$ and $Q^*_{mBk}$.

It proved to be more convenient in the actual calculation procedure to sum Eqs (26) and (27) over $m$ first and then over $k$. The convergence properties of the double sums could be monitored more easily this way. Convergence of the double sums is excellent over most of the blade, but becomes less rapid as the leading and trailing edges are approached. Also, $u_s$ converged slightly faster than $u_n$. A slow convergence rate near the leading and trailing edges is not unexpected because it is known that, in the linear approximation, a biconvex parabolic arc airfoil section has logarithmic singularities in $u_s$ at the edges. Nevertheless, except very close to the edges, excellent convergence has been obtained in the cases considered with the double sums truncated at a maximum $k$ of 7 and a maximum $m$ of 15 to 20.

## 3. COMPUTED RESULTS

Calculations have been carried out for two sample cases. The geometrical and operating parameters chosen were a blade number, $B$, of 64; a hub radius to tip radius ratio, $h$, of 0.9; a solidity, $C_a/L_T$, of 0.5; an axial Mach number, $M$, of 0.6; and two values of the ratio of tip speed to undisturbed sound speed, $M_T$, namely 0.529 and 0.775 which give resultant relative tip Mach numbers, $M_R$, of 0.80 and 0.98, respectively. The solidity used here is defined as the projection of the chord on the axial direction, $C_a$, divided by the spacing between the blade tips, $L_T$, where $L_T = 2\pi r_T/B$. Also, the same thickness ratio variation used by McCune,

$$\tau(\rho) = \tau_o \frac{\rho_H}{\rho} \frac{\sqrt{1+\rho_H^2}}{\sqrt{1+\rho^2}} \tag{28}$$

was assumed. This $\tau(\rho)$ varies nearly linearly with radius from a value $\tau_o$ at the hub to tip values of $0.844\,\tau_o$ for $M_R = 0.80$ and $0.860\,\tau_o$ for $M_R = 0.98$.

Chordwise distributions of normalized pressure coefficient, $C_p/\tau_o$, are presented in Fig. 3 for $M_R = 0.98$ at three radial stations. The pressure is symmetrical about midchord for the symmetrical thickness. The corresponding computations from Ref 2 are presented for comparison, along with the strip (cascade) theory distribution at the blade tip, also from Ref 2. The differences between the present results and those of Ref 2 have not been resolved. Differences also exist for $M_R = 0.80$, but in that case the present results lie slightly above McCune's. As a check on the procedure used here, $u_s$ was computed alternately by numerically differentiating the potential in the same way as in Ref 2. The results were identical to those computed directly from Eq (26). It is suspected, therefore, that the discrepancies arise from the different procedures used for computing $K_{mBk}$ and $Q^*_{mBk}$.

Chordwise distributions of the mean blade surface ordinates $\eta$, nondimensionalized by $c\tau_o$, where $c$ is the local chord which varies with the radius for a constant $c_a$, are presented at three radial stations in Fig. 4 for $M_R = 0.80$ and in Fig. 5 for $M_R = 0.98$. The blade mean surface shapes consist of a negative incidence angle plus a camber distribution which is antisymmetric about midchord for the symmetrical thickness distribution considered here. Comparison of the two cases indicates that as $M_R$ increases toward unity the incidence angle becomes slightly more negative and the amount of camber becomes slightly more positive.

There is very little difference from one radius to the next especially for the example in Fig. 4 where the blade ordinates are virtually indistinguishable from one another. This indicates that three-dimensional effects may not be of great importance for these cases. It would be instructive to make a strip (cascade) calculation of the mean blade surface ordinates to establish the three-dimensional effects, but this has not been carried out. When $M_R$ increases to supersonic values, however, it is expected that three-dimensional effects will be significant, just as they are in the pressure distributions, as McCune demonstrated in Ref 2.

# IV. FLOW FIELD WITHIN BLADE ROW DUE TO BLADE LIFT

## 1. SUMMARY OF BASIC ANALYSIS

Recently, Okurounmu and McCune (Refs 3 and 4) have extended McCune's earlier analysis to describe the linearized, three-dimensional flow through a lifting blade row. Their analysis for the lifting case is partly based on the earlier work of Reissner (Ref 16) and Davidson (Ref 17). Reissner examined the linearized, incompressible flow through a propeller in free air. His basic approach was to solve for the velocity potential in the far wake, using a source distribution to obtain the required discontinuity at the trailing helical vortex sheets far behind the blades. The blades were represented by vortex lines having bound circulation $\Gamma(\rho)$ . Reissner found a source distribution which would produce the required discontinuity, $\Gamma(\rho)$ , in the velocity potential at the blade wakes. He then had to add another source distribution to cancel the unwanted effects of the first, off the wakes. This enabled him to compute the induced velocities due to the vortex lines and their associated wakes of trailing vorticity. Davidson extended Reissner's solution to the case of a propeller in a wind tunnel including compressibility effects. It should be mentioned that Reissner's results have been obtained by other investigators using different procedures, for example, see Lerbs' derivation in Appendix 1 of Ref 18.

The governing equation for the linearized flow through a lifting blade row in an infinite annulus is Eq (1), which in the far wake reduces to

$$\frac{1}{\rho}\,\frac{\partial}{\partial \rho}\left(\rho\,\frac{\partial \varphi}{\partial \rho}\right) + \left(1+\frac{1}{\rho^2}\right)\frac{\partial^2 \varphi}{\partial \zeta^2} = 0 \tag{29}$$

where $\zeta = \theta - z$ as before. This is the same equation for the wake potential that Reissner solved. Accounting for the presence of the hub and the shroud, where the radial velocity must vanish, Okurounmu and McCune obtain the following result for the wake potential

$$\varphi_w = \frac{B}{2\pi}\left[\Gamma(\rho)\,\zeta_\ell - 2\sum_{m=1}^{\infty}\frac{1}{mB}\,\alpha_m(\rho)\,\sin\,(mB\zeta)\right] \tag{30}$$

where $B$ is again the number of blades, $\zeta_\ell = \zeta - \frac{(2\ell+1)\pi}{B}, \ell = 0, 1, \ldots, (B-1)$, and varies linearly from $-\frac{\pi}{B}$ to $+\frac{\pi}{B}$ between adjacent blades. The blades are located at $\zeta = \frac{2j\pi}{B}$, $j = 0, 1, \ldots, (B-1)$, and

$$\chi_m(\rho) = \frac{K'(\rho_T)\, I'(\rho_H)\, K(\rho) - K'(\rho_T) K'(\rho_H)\, I(\rho)}{Z(\rho_H, \rho_T)} \int_{\rho_H}^{\rho_T} \xi \frac{dI}{d\xi} \frac{d\Gamma}{d\xi} d\xi$$

$$+ \frac{I'(\rho_T) K'(\rho_H)\, I(\rho) - I'(\rho_T) I'(\rho_H)\, K(\rho)}{Z(\rho_H, \rho_T)} \int_{\rho_H}^{\rho_T} \xi \frac{dK}{d\xi} \frac{d\Gamma}{d\xi} d\xi$$

$$+ I(\rho) \int_{\rho_H}^{\rho} \xi \frac{dK}{d\xi} \frac{d\Gamma}{d\xi} d\xi - K(\rho) \int_{\rho_H}^{\rho} \xi \frac{dI}{d\xi} \frac{d\Gamma}{d\xi} d\xi \tag{31}$$

where $I(\rho)$ and $K(\rho)$ are abbreviated notations for $I_{mB}(mB\rho)$ and $K_{mB}(mB\rho)$, the modified Bessel functions of the first and second kind and order $mB$, and

$$Z = K'(\rho_T)\, I'(\rho_H) - K'(\rho_H)\, I'(\rho_T) \tag{32}$$

The solution for the complete potential downstream of the rotor was obtained by adding particular solutions in the form of Eq (2) and the additional particular solution $\bar{\Gamma} z$ to the wake solution where

$$\bar{\Gamma} = \frac{2}{(1-h^2)\rho_T^2} \int_{\rho_H}^{\rho_T} \Gamma(\rho)\, \rho\, d\rho \tag{33}$$

The particular solution is needed because $\phi_w$ plus a general function of $z$ satisfies Eq (1). Upstream only the particular solutions in the form of Eq (2) are needed. Matching the potential and the mass flow at the rotor plane, Okurounmu and McCune obtain the following solution for the velocity potential due to $B$ vortex lines rotating in an infinite annulus, real part implied,

$$\varphi^{u} = \frac{B}{2\pi\beta^2}\left\{-\sum_{k=1}^{\infty}\frac{\Gamma_{ok}}{2\lambda_{ok}}\,e^{\lambda_{ok}z}\,R_o\left(K_{ok}\frac{\rho}{\rho_T}\right)\right.$$

$$\left.+\sum_{m=1}^{\infty}\sum_{k=1}^{\infty}\left[\frac{i}{mB}\,\beta^2\left(\Gamma_{mk}+H_{mk}\right)+\frac{H_{mk}}{\lambda_{mBk}}\right]\,e^{imB\theta}\,e^{\left(imB\frac{M^2}{\beta^2}+\lambda_{mBk}\right)z}\,R_{mB}\left(K_{mBk}\frac{\rho}{\rho_T}\right)\right\}$$

$$\varphi^{\alpha} = \frac{B}{2\pi\beta^2}\left\{\bar{\Gamma}z+\beta^2\Gamma(\rho)\,\zeta_{\ell}-\sum_{k=1}^{\infty}\frac{\Gamma_{ok}}{2\lambda_{ok}}\,e^{-\lambda_{ok}z}\,R_o\left(K_{ok}\frac{\rho}{\rho_T}\right)\right. \qquad (34)$$

$$+\beta^2\sum_{m=1}^{\infty}\sum_{k=1}^{\infty}\frac{2i}{mB}\,H_{mk}\,e^{imB\zeta}\,R_{mB}\left(K_{mBk}\frac{\rho}{\rho_T}\right)$$

$$\left.+\sum_{m=1}^{\infty}\sum_{k=1}^{\infty}\left[-\frac{i\beta^2}{mB}\left(\Gamma_{mk}+H_{mk}\right)+\frac{H_{mk}}{\lambda_{mBk}}\right]e^{imB\theta}\,e^{\left(imB\frac{M^2}{\beta^2}-\lambda_{mBk}\right)z}\,R_{mB}\left(K_{mBk}\frac{\rho}{\rho_T}\right)\right\}$$

where $\Gamma(\rho)$ is the bound circulation and the quantities $\Gamma_{ok}$, $\Gamma_{mk}$, and $H_{mk}$ are coefficients in the expansions

$$\Gamma = \bar{\Gamma}+\sum_{k=1}^{\infty}\Gamma_{ok}\,R_o\left(K_{ok}\frac{\rho}{\rho_T}\right) \qquad (35a)$$

$$\Gamma = \sum_{k=1}^{\infty}\Gamma_{mk}\,R_{mB}\left(K_{mBk}\frac{\rho}{\rho_T}\right) \qquad (35b)$$

$$\chi_m(\rho) = \sum_{k=1}^{\infty}H_{mk}\,R_{mB}\left(K_{mBk}\frac{\rho}{\rho_T}\right) \qquad (35c)$$

The inclusion of $\bar{\Gamma}$ in the solution is seen to be required because the $R_o\left(K_{ok}\frac{\rho}{\rho_T}\right)$ do not form a complete set.

This solution was used by Okurounmu and McCune in Ref 3 to compute the induced drag for a rotor at high subsonic tip speeds. However, these results cannot be used at supersonic tip speeds because, as they point out, a vortex line has infinite wave drag in supersonic flow. Later, in Ref 4, Okurounmu and McCune extend the above result to cover a lifting surface

model for the rotor blades. With this model, a finite wave drag can be obtained.

In deriving the lifting surface result, the solution for single vortex lines is used as the potential due to an elementary strip of blade surface. Then, by distributing elementary strips of bound circulation over a helical blade surface and integrating across the chord, the lifting surface result is obtained. For the special case where the vortex strength, $\gamma(\rho, \xi)$, can be factored, i.e.

$$\gamma(\rho, \xi) = \frac{\Gamma(\rho)\, g_2\, \xi}{\sqrt{1+\rho^2}} \tag{36}$$

where

$$\Gamma(\rho) = \int_0^{c_a} \gamma(\rho, \xi) \sqrt{1+\rho^2}\, d\xi \tag{37}$$

$$\int_0^{c_a} g_2(\xi)\, d\xi = 1 \tag{38}$$

and $c_a$ is the constant projection of the chord on the axis, the quantities $\Gamma_{ok}$, $\Gamma_{mk}$, and $H_{mk}$ have the same meaning as in the concentrated bound vortex solution. For this case, the lifting surface result for the velocity potential is, the real part implied,

$$\varphi^u = \frac{B}{2\pi\beta^2}\left\{-\sum_{k=1}^{\infty} \frac{G^u_{ok}\,\Gamma_{ok}}{2\lambda_{ok}}\, e^{\lambda_{ok} z}\, R_o\left(K_{ok}\frac{\rho}{\rho_T}\right) + \sum_{m=1}^{\infty}\sum_{k=1}^{\infty}\left[\frac{i}{mB}\,\beta^2(\Gamma_{mk}+H_{mk})\right. \right. \tag{39}$$

$$\left. \left. + \frac{H_{mk}}{\lambda_{mBk}}\right] G^u_{mk}\, e^{imB\theta}\, e^{\left(i\frac{mBM^2}{\beta^2}+\lambda_{mBk}\right)z}\, R_{mB}\left(K_{mBk}\frac{\rho}{\rho_T}\right)\right\}$$

$$\varphi^{d} = \frac{B}{2\pi\beta^2}\left\{\bar{\Gamma}\int_0^{c_a} g_2(\xi)\left(z - \frac{\omega\xi}{U}\right)d\xi + \beta^2\Gamma\zeta_\ell - \sum_{k=1}^{\infty}\frac{G_{ok}^{d}\Gamma_{ok}}{2\lambda_{ok}}e^{-\lambda_{ok}z}R_o\left(K_{ok}\frac{\rho}{\rho_T}\right)\right.$$

$$+\beta^2\sum_{m=1}^{\infty}\sum_{k=1}^{\infty}\frac{2i}{mB}H_{mk}e^{imB\zeta}R_{mB}\left(K_{mBk}\frac{\rho}{\rho_T}\right)+\sum_{m=1}^{\infty}\sum_{k=1}^{\infty}\left[-\frac{i\beta^2}{mB}\left(\Gamma_{mk}+H_{mk}\right)\right.$$

$$\left.\left.+\frac{H_{mk}}{\lambda_{mBk}}\right]G_{mk}^{d}e^{imB\theta}e^{\left(imB\frac{M^2}{\beta^2}-\lambda_{mBk}\right)z}R_{mB}\left(K_{mBk}\frac{\rho}{\rho_T}\right)\right\} \tag{40}$$

$$\varphi^{i} = \frac{B}{2\pi\beta^2}\left\{\bar{\Gamma}\int_0^{x} g_2(\xi)\left(z - \frac{\omega\xi}{U}\right)d\xi + \beta^2\Gamma\zeta_\ell\int_0^{x} g_2(\xi)\,d\xi\right.$$

$$-\sum_{k=1}^{\infty}\frac{\Gamma_{ok}}{2\lambda_{ok}}\left[G_{ok}^{1}e^{-\lambda_{ok}z}+G_{ok}^{2}e^{\lambda_{ok}z}\right]R_o\left(K_{ok}\frac{\rho}{\rho_T}\right)$$

$$+\beta^2\sum_{m=1}^{\infty}\sum_{k=1}^{\infty}\frac{2i}{mB}H_{mk}e^{imB\zeta}R_{mB}\left(K_{mBk}\frac{\rho}{\rho_T}\right)\int_0^{x} g_2(\xi)\,d\xi$$

$$+\sum_{m=1}^{\infty}\sum_{k=1}^{\infty}\left[-\frac{i\beta^2}{mB}\left(\Gamma_{mk}+H_{mk}\right)+\frac{H_{mk}}{\lambda_{mBk}}\right]e^{imB\theta}e^{\left(\frac{imBM^2}{\beta^2}-\lambda_{mBk}\right)z}G_{mk}^{1}R_{mB}\left(K_{mBk}\frac{\rho}{\rho_T}\right)$$

$$\left.+\sum_{m=1}^{\infty}\sum_{k=1}^{\infty}\left[+\frac{i\beta^2}{mB}\left(\Gamma_{mk}+H_{mk}\right)+\frac{H_{mk}}{\lambda_{mBk}}\right]e^{imB\theta}e^{\left(\frac{imBM^2}{\beta^2}+\lambda_{mBk}\right)z}G_{mk}^{2}R_{mB}\left(K_{mBk}\frac{\rho}{\rho_T}\right)\right\} \tag{41}$$

where

$$G_{ok}^{u,d} = \int_0^{c_a} g_2(\xi)\,e^{\mp\lambda_{ok}\frac{\omega\xi}{U}}\,d\xi \tag{42}$$

$$G_{mk}^{u,d} = \int_0^{c_a} g_2(\xi)\,e^{-\left(\frac{imB}{\beta^2}\pm\lambda_{mBk}\right)\frac{\omega\xi}{U}}\,d\xi \tag{43}$$

$$G^1_{mk} = \int_0^x e^{-imB\frac{\omega\xi}{U}} e^{-\left(\frac{imBM^2}{\beta^2} - \lambda_{mBk}\right)\frac{\omega\xi}{U}} q_2(\xi)\, d\xi \tag{44}$$

$$G^2_{mk} = \int_x^{c_a} e^{-imB\frac{\omega\xi}{U}} e^{-\left(\frac{imBM^2}{\beta^2} + \lambda_{mBk}\right)\frac{\omega\xi}{U}} q_2(\xi)\, d\xi \tag{45}$$

The perturbation pressure, disturbance velocities and mean blade surface ordinates can be obtained again by Eqs (11) to (18). Examination of Eqs (39) to (41) shows that there are acoustic modes which are either propagated undamped, or damped rapidly depending on whether or not $\lambda_{mBk}$ is imaginary. The cutoff criterion is identical to that for the thickness case.

A particularly interesting feature of the above solution is that there is no transonic resonance for the case of constant work design, that is, when the bound circulation is independent of radius. In this case there is no trailing vorticity and the Reissner wake functions, $\chi_m(\rho)$, vanish. Hence, in the expressions for the potential, the quantities $H_{mk}$ all vanish and the amplitudes of the propagating duct modes no longer contain a term inversely proportional to $\lambda_{mBk}$.

The hub thickness-to-chord ratio $\tau_0$ has been used above as a physically significant small parameter in the thickness case. A physically significant small parameter is required in the lifting case, too, and to this end, it is useful to consider the circumferential average of the total pressure rise across the blade row in duct-fixed coordinates, $R_\infty$, say, which was shown in Ref 3 to be given by

$$R_\infty(\rho) \equiv \frac{\langle\langle p_0(\rho)\rangle\rangle_{z=+\infty}}{\langle\langle p_0\rangle\rangle_{z=-\infty}} = 1 - \frac{\bar{\gamma} M^2 \omega B \Gamma(\rho)}{2\pi U^2 \left(1 + \frac{\bar{\gamma}-1}{2} M^2\right)} \tag{46}$$

where $\bar{\gamma}$ is the ratio of specific heats. Note that $\Gamma$ is negative when work is done on the fluid so that the total pressure rise is positive. As indicated in Eq (46), this relationship holds at each radius. In the special case of constant work design, which will be considered subsequently in this report, $\Gamma$ is constant and so $R_\infty$ is constant everywhere in the annulus. If a normalized total

pressure rise factor $\sigma_\infty$ is defined by

$$\sigma_\infty \equiv R_\infty - 1 \tag{47}$$

then

$$\Gamma = -\frac{2\pi U^2\left(1+\frac{\bar\gamma-1}{2}M^2\right)}{\bar\gamma M^2 \omega B}\,\sigma_\infty \tag{48}$$

and $\sigma_\infty$ is the suitable small parameter. The quantities $\Gamma_{mk}$ in Eq (35b) can be written now as

$$\Gamma_{mk} = -\frac{2\pi U^2\left(1+\frac{\bar\gamma-1}{2}M^2\right)\sigma_\infty}{\bar\gamma M^2 \omega B}\,\Gamma^*_{mk} \tag{49}$$

where

$$\Gamma^*_{mk} = \int_k^1 R_{mB}\left(K_{mBk}\frac{\rho}{\rho_T}\right)\frac{\rho}{\rho_T}\,d\left(\frac{\rho}{\rho_T}\right) \tag{50}$$

The specification of the blade loading must be completed by specifying the chordwise distribution, i.e. the $g_2(\xi)$ in Eq (36). In the present report a constant chordwise distribution has been assumed, which by Eq (38) must be

$$g_2(\xi) = \frac{1}{c_a} \tag{51}$$

This uniform distribution is the $a = 1$ mean line loading that is one case of the NACA 6-series wing sections, see pp 119 to 122 of Ref 19.

The streamwise, $u_s$, and normal, $u_n$, components of the induced velocity anywhere within the blade row can be found in the uniform chordwise loading, constant work case by evaluating Eqs (12) and (14) by means of Eqs (41), (44), (45) and (49) to (51). The results are

$$\frac{u_s}{U_o\sigma_\infty} = -\frac{\left(1+\frac{\bar\gamma-1}{2}M^2\right)}{\bar\gamma M^2 \delta_x}\left\{\frac{1}{(1+\rho^2)}\left(\frac{z}{\beta^2}+\zeta_l\right)+\sum_{m=1}^{\infty}\sum_{k=1}^{\infty}L_{mk}(\rho)\left[S^c_{mk}(z)\cos mB\zeta + S^s_{mk}(z)\sin mB\zeta\right]\right\} \tag{52}$$

$$\frac{u_n}{U_o \sigma_\infty} = -\rho\left[\frac{u_s}{U_o \sigma_\infty}\right] - \frac{\left(1+\frac{\bar{\gamma}-1}{2}M^2\right)}{\bar{\gamma} M^2 \delta_\chi}\left\{\frac{z}{\rho} - \sum_{m=1}^{\infty}\sum_{k=1}^{\infty}\frac{mB(1+\rho^2)}{\rho} L_{mk}(\rho)\left[N^c_{mk}(z)\cos mB\zeta\right.\right.$$

$$\left.\left. + N^s_{mk}(z)\sin mB\zeta\right]\right\} \qquad (53)$$

where

$$L_{mk}(\rho) = \frac{\Gamma^*_{mk} R_{mB}(K_{mBk}\frac{\rho}{\rho_T})}{mB(1+\rho^2)}, \qquad m \geq 1 \qquad (54)$$

$$\delta_\chi = \omega c_a / U \qquad (55)$$

The quantities $\mathcal{S}^c_{mk}$, etc. are different from the quantities with the same notation in the thickness case. Again they are functions of $z$ only and have different forms depending on whether or not the $\lambda_{mBk}$ are real. Attention in this report is concentrated on subsonic relative tip Mach numbers for which all $\lambda_{mBk}$ are real. The appropriate values of $\mathcal{S}^c_{mk}$, etc. are given in Table II.

Evaluation of the blade mean surface pressure distribution and ordinates requires expressions for $u_s$ and $u_n$ on the linearized location of the mean surface, namely $n = 0$, i.e., $\zeta = \theta - z = \frac{2j\pi}{B}$, $j = 0, 1, \ldots, (B-1)$. If Eq (52) for $u_s$ is considered first, it can be shown that the $\zeta_\ell$ term provides a jump in tangential velocity, $\Delta u_s = u_s(r, n=0+, s) - u_s(r, n=0-, s)$, across the blade surface as it is approached from above and below. That is, using Eqs (36), (48) and (51) it follows that

$$\Delta u_s = -\gamma \qquad (56)$$

The remaining terms in Eq (52) are continuous across the mean blade surface including the double sum. Therefore, taking the value of $\zeta$ at the blade surface, namely zero, the portion of $u_s$ that is continuous across the blade surface is

$$\frac{u_s(r, n=0, s)}{U_o \sigma_\infty} = -\frac{\left(1+\frac{\bar{\gamma}-1}{2}M^2\right)}{\bar{\gamma} M^2 \delta_\chi}\left\{\frac{z}{(1+\rho^2)\beta^2} + \sum_{m=1}^{\infty}\sum_{k=1}^{\infty} L_{mk}(\rho)\,\mathcal{S}^c_{mk}(z)\right\} \qquad (57)$$

The normal component in Eq (53) is continuous across the mean blade surface, and is given by

$$\frac{u_n(r,n=0,s)}{U_0\sigma_\infty} = -\rho\left[\frac{u_s(r,n=0,s)}{U_0\sigma_\infty}\right] - \frac{\left(1+\frac{\bar\gamma-1}{2}M^2\right)}{\bar\gamma M^2 \delta_x}\left\{\frac{z}{\rho}\right. \\ \left. - \sum_{m=1}^{\infty}\sum_{k=1}^{\infty}\frac{mB(1+\rho^2)}{\rho} L_{mk}(\rho) N^c_{mk}(z)\right\} \tag{58}$$

The blade mean surface ordinates may then be found by integrating Eq (18) with Eq (58).

## 2. METHOD OF COMPUTATION

The loading case is very similar to the thickness case from the computational point of view, as can be seen by comparing Eqs (25) to (27) and Eqs (54), (57) and (58). The principal task again is the evaluation of $K_{mBk}$ and $\Gamma^*_{mk}$ which is carried out by a slight modification of the computer program for evaluating $K_{mBk}$ and $Q^*_{mk}$. For fixed values of $B$ and $k$ and for a uniform chordwise loading, the $\Gamma^*_{mk}$ can be calculated once and for all, see Eq (50).

A separate computer program has been written to evaluate $u_s/U_0\sigma_\infty$, $u_n/U_0\sigma_\infty$, $C_p/\sigma_\infty$ and $\eta/c\sigma_\infty$. The input required is $K_{mBk}$ and $\Gamma^*_{mk}$ from the first program as well as the compressor operating conditions. In the loading case a subroutine has been added to integrate Eq (18).

Convergence properties of the double sums are similar to the thickness case. A constant chordwise loading distribution gives rise to logarithmic singularities in $u_n$ at the leading and trailing edges, but these singularities are integrable to obtain the blade ordinates, see pp 73-75 of Ref 19. Overall, except near the edges, excellent convergence was achieved in the examples considered with the double sums truncated at a maximum $k$ of 7 and a maximum $m$ of 10.

## 3. COMPUTED RESULTS

Calculations have been carried out for two sample cases with the same

conditions as the thickness cases in the previous section. That is, the conditions are $B = 64$, $h = 0.9$, $C_a/L_T = 0.5$, $M = 0.6$ and the two values of $M_T$, namely 0.529 and 0.775 which give $M_R$ values of 0.80 and 0.98, respectively.

Chordwise distributions of that portion of the normalized pressure coefficient, $\hat{C}_p/\sigma_\infty$, that is symmetrical above and below the blade mean surface, from Eqs (17) and (57), are presented in Fig. 6 for $M_R = 0.98$ at three radial stations. The pressure is made up of a linear contribution from the first term in Eq (57) and a double sum contribution that is antisymmetrical about midchord for the uniform chordwise loading. Although not presented here, the corresponding results for $M_R = 0.80$ differ from those in Fig. 6 by less than 10 percent everywhere. The differences are in a direction to reduce the slope of $\hat{C}_p/\sigma_\infty$ as $M_R$ increases. It would be instructive in this case to carry out a strip (cascade) calculation of the symmetrical part of the pressure distribution to establish the three dimensional effects. However, just as in the thickness case, this has not been carried out as yet.

Chordwise distributions of the mean blade surface ordinates $\eta$, nondimensionalized by $c\sigma_\infty$, are presented at three radial stations in Fig. 7 for $M_R = 0.80$ and in Fig. 8 for $M_R = 0.98$. The blade mean surface shapes in the lifting case consist of a positive incidence angle plus a camber distribution which is symmetrical about midchord for uniform chordwise loading. The camber shape is generally similar to that for two-dimensional airfoils with uniform chordwise loading, see the $a = 1$ mean line results in Ref 19. The incidence angle and amount of camber decrease from hub to tip and also decrease markedly as $M_R$ increases.

McCune and Okurounmu have published blade shape results recently in Ref 4. Their computational scheme differs from the present one although the basic analysis is the same. Corresponding cases should be examined using the present scheme so that direct comparisons can be made, but this has not been done as yet. Nevertheless it is shown in Ref 4 that the blade mean surface ordinates at any radius go to zero when the relative Mach number is unity at that radius and this appears to be the trend of the calculations made here.

# V. CONCLUDING REMARKS

Analyses have been carried out for calculation of the velocity and pressure fields within a blade row operating in an infinite annulus at transonic Mach numbers of the flow relative to the blades. In addition, the relationship between the induced velocity and the blade mean surface shapes has been determined. It has been established that the effects of a specified blade thickness distribution can be separated from the effects of a specified distribution of blade lift. A computational scheme has been developed and used to evaluate the blade mean surface ordinates and pressure distributions for cases in which the relative flow velocity incident to the blade tips has a high subsonic Mach number.

In the thickness case, blade surface pressure distributions have been calculated in two examples for blades with biconvex parabolic arc sections of radially tapering thickness. McCune had previously computed pressures for these examples by means of the same basic analysis, but with a different computational scheme. Certain differences between the present results and those of McCune still require resolution. Blade mean surface shapes which will insure that the blades are locally nonlifting have been calculated for the first time and are given for the two examples. These results should be examined more fully, particularly with respect to the three-dimensional effects.

Extension of the analysis and computational procedures to examples for which the relative tip Mach number is supersonic (retaining a subsonic axial Mach number) is straightforward and should be undertaken. Not only is this transonic case of interest with respect to blade row performance, but it is of great significance from the acoustic point of view. Acoustic energy is radiated from a single blade row only at supersonic relative tip speeds, as discussed by Lordi, so that determination of the corresponding blade mean surface shapes would complete the relationship between detailed blade geometry and acoustic intensity.

In the lifting case, the portions of the blade surface pressure distributions

that are symmetrical above and below the blade mean surface have been calculated in two examples for blades with a uniform chordwise loading and a constant work spanwise loading. These results, which have also been obtained for the first time, require further attention to clarify the nature of the three-dimensional effects. Blade mean surface shapes that are necessary to achieve the specified blade loading have been calculated in the same two examples. McCune and Okurounmu have also computed blade mean surface shapes but again with a different computational scheme. Corresponding calculations should be made by the present techniques to provide direct comparisons. It is also important to generalize the present analysis and computational scheme to account for other chordwise and radial distributions of blade loadings. Extension to supersonic relative tip speeds should be carried out as well to complete the relationship between the detailed blade geometry and the acoustic intensity in the lifting case.

The relative magnitudes of the blade mean surface ordinates due to thickness and lift are comparable for similar values of hub thickness-to-chord ratio and the total pressure rise parameter. In particular, as the relative Mach number at the tip approaches unity and the incidence angle and camber due to lift decrease greatly, the principal contribution to the blade shape arises from the thickness. Therefore, thickness plays an important role in practical blade shape design.

## REFERENCES


1. McCune, J.E., "A Three-Dimensional Theory of Axial Compressor Blade Rows-Application in Subsonic and Supersonic Flows," Journal of the Aerospace Sciences, Vol. 25, No. 9, Sept. 1958, pp. 544-560.

2. McCune, J.E., "The Transonic Flow Field of an Axial Compressor Blade Row," Journal of the Aerospace Sciences, Vol. 25, No. 10, Oct. 1958, pp. 616-626.

3. Okurounmu, O. and McCune, J.E., "Three-Dimensional Vortex Theory of Axial Compressor Blade Rows at Subsonic and Transonic Speeds," AIAA Journal, Vol. 8, No. 7, July 1970, pp. 1275-1283.

4. Okurounmu, O. and McCune, J.E., "Transonic Lifting Surface Theory for Axial Flow Compressors," United Aircraft Research Laboratories Report K213580-1, March 1971.

5. Lordi, J.A., "Report on a Study of Noise Generation by a Rotating Blade Row in an Infinite Annulus," U.S. Air Force Office of Scientific Research Scientific Report AFOSR TR-71-1485 (also available as Cornell Aeronautical Laboratory, Inc. Report AI-2836-A-1), May 1971.

6. Lordi, J.A., "Noise Generation by a Rotating Blade Row in an Infinite Annulus," AIAA Paper No. 71-617, AIAA 4th Fluid and Plasma Dynamics Conference, Palo Alto, California, June 21-23, 1971.

7. Tyler, J.M. and Sofrin, T.G., "Axial Flow Compressor Noise Studies," SAE Transactions, Vol. 70, 1962, pp. 309-332.

8. Lowson, M.V., "Theoretical Studies of Compressor Noise," NASA CR-1287, March 1969.

9. Mani, R., "Discrete Frequency Noise Generation from an Axial Flow Fan Blade Row," ASME Paper No. P-69-FE-12 presented at the Applied Mechanics Conference, Evanston, Illinois, June 16-18, 1969.

10. Slutsky, M., "Discrete Noise Generation and Propagation by a Fan Engine," Proceedings of AFOSR-UTIAS Symposium on Aerodynamic Noise, Toronto, May 20-21, 1968, pp. 331-349.

11. Thwaites, B., Editor, "Incompressible Aerodynamics," Oxford University Press, London, 1960.

12. Robinson, A. and Laurmann, J.A., "Wing Theory," Cambridge University Press, Cambridge, 1956.

13. Kerwin, J.E. and Leopold, R., "A Design Theory for Subcavitating Propellers," Transactions, Society of Naval Architects and Marine Engineers, Vol. 72, 1964, pp. 294-335.

14. Kerwin, J.E. and Leopold, R., "Propeller-Incidence Corrections due to Blade Thickness," Journal of Ship Research, Vol. 7, No. 2, October 1963, pp. 1-6.

15. Olver, F.W.J., "The Asymptotic Expansion of Bessel Functions of Large Order," Philosophical Transactions of the Royal Society of London, Series A, Vol. 247, 1954, pp. 328-368.

16. Reissner, H., "On the Vortex Theory of the Screw Propeller," Journal of the Aeronautical Sciences, Vol. 5, No. 1, Nov. 1937, pp. 1-7.

17. Davidson, R.E., "Linearized Potential Theory of Propeller Induction in a Compressible Flow," NACA TN 2983, Sept. 1953.

18. Lerbs, H., "Moderately Loaded Propellers with a Finite Number of Blades and an Arbitrary Distribution of Circulation," Transactions, Society of Naval Architects and Marine Engineers, Vol. 60, 1952, pp. 73-123.

19. Abbott, I.H. and Von Doenhoff, A.E., "Theory of Wing Sections," Dover Publications, Inc., New York, 1959.

TABLE I

VALUES OF $S^c_{mk}, S^s_{mk}, N^c_{mk}, N^s_{mk}$ FOR SUBSONIC RELATIVE TIP SPEEDS
THICKNESS CASE, BICONVEX, PARABOLIC ARC SECTION

$$S^c_{ok}(z) = -\frac{2}{\lambda^2_{ok}\delta_x} + \frac{e^{-\lambda_{ok}z}}{2\lambda_{ok}}\left(1+\frac{2}{\lambda_{ok}\delta_x}\right) + \frac{e^{-\lambda_{ok}(\delta_x - z)}}{2\lambda_{ok}}\left(1+\frac{2}{\lambda_{ok}\delta_x}\right)$$

$$S^c_{mk}(z) = \frac{1}{\lambda_{mBk}\left[\lambda^2_{mBk}+\left(\frac{mB}{\beta^2}\right)^2\right]}\left\{-\frac{4\lambda_{mBk}}{\delta_x} + \left[\lambda^2_{mBk}+\left(\frac{mB}{\beta^2}\right)^2\right]\left[e^{-\lambda_{mBk}z}\cos\frac{mBz}{\beta^2} + e^{-\lambda_{mBk}(\delta_x - z)}\cos\frac{mB(\delta_x - z)}{\beta^2}\right]\right.$$

$$+\frac{2}{\delta_x}\left[\lambda_{mBk}e^{-\lambda_{mBk}z}\cos\frac{mBz}{\beta^2} - \left(\frac{mB}{\beta^2}\right)e^{-\lambda_{mBk}z}\sin\frac{mBz}{\beta^2} + \lambda_{mBk}e^{-\lambda_{mBk}(\delta_x - z)}\cos\frac{mB(\delta_x - z)}{\beta^2}\right.$$

$$\left.\left. - \left(\frac{mB}{\beta^2}\right)e^{-\lambda_{mBk}(\delta_x - z)}\sin\frac{mB(\delta_x - z)}{\beta^2}\right]\right\} \quad , \qquad m \geq 1$$

$$S^s_{ok}(z) = 0$$

$$S^s_{mk}(z) = -\frac{1}{\lambda_{mBk}\left[\lambda^2_{mBk}+\left(\frac{mB}{\beta^2}\right)^2\right]}\left\{\left[\lambda^2_{mBk}+\left(\frac{mB}{\beta^2}\right)^2\right]\left[e^{-\lambda_{mBk}z}\sin\frac{mBz}{\beta^2} - e^{-\lambda_{mBk}(\delta_x - z)}\sin\frac{mB(\delta_x - z)}{\beta^2}\right]\right.$$

$$+\frac{2}{\delta_x}\left[\lambda_{mBk}e^{-\lambda_{mBk}z}\sin\frac{mBz}{\beta^2} + \left(\frac{mB}{\beta^2}\right)e^{-\lambda_{mBk}z}\cos\frac{mBz}{\beta^2} - \lambda_{mBk}e^{-\lambda_{mBk}(\delta_x - z)}\sin\frac{mB(\delta_x - z)}{\beta^2}\right.$$

$$\left.\left. - \left(\frac{mB}{\beta^2}\right)e^{-\lambda_{mBk}(\delta_x - z)}\cos\frac{mB(\delta_x - z)}{\beta^2}\right]\right\} \quad , \qquad m \geq 1$$

TABLE I (concluded)

$$N^{c}_{mk}(z) = \frac{1}{\lambda_{mBk}\left[\lambda^{2}_{mBk}+\left(\frac{mB}{\beta^{2}}\right)^{2}\right]}\left\{\frac{\delta\lambda_{mBk}\left(\frac{mB}{\beta^{2}}\right)}{\delta_{\chi}\left[\lambda^{2}_{mBk}+\left(\frac{mB}{\beta^{2}}\right)^{2}\right]} - e^{-\lambda_{mBk}z}\left[\lambda_{mBk}\sin\frac{mBz}{\beta^{2}}+\frac{mB}{\beta^{2}}\cos\frac{mBz}{\beta^{2}}\right]\right.$$

$$-e^{-\lambda_{mBk}(\delta_{\chi}-z)}\left[\lambda_{mBk}\sin\frac{mB(\delta_{\chi}-z)}{\beta^{2}}+\frac{mB}{\beta^{2}}\cos\frac{mB(\delta_{\chi}-z)}{\beta^{2}}\right]-\frac{2e^{-\lambda_{mBk}z}}{\delta_{\chi}\left[\lambda^{2}_{mBk}+\left(\frac{mB}{\beta^{2}}\right)^{2}\right]}\left\{\left[\lambda^{2}_{mBk}\right.\right.$$

$$\left.-\left(\frac{mB}{\beta^{2}}\right)^{2}\right]\sin\frac{mBz}{\beta^{2}}+2\lambda_{mBk}\left(\frac{mB}{\beta^{2}}\right)\cos\frac{mBz}{\beta^{2}}\Big]-\frac{2e^{-\lambda_{mBk}(\delta_{\chi}-z)}}{\delta_{\chi}\left[\lambda^{2}_{mBk}+\left(\frac{mB}{\beta^{2}}\right)^{2}\right]}\left\{\left[\lambda^{2}_{mBk}\right.\right.$$

$$\left.\left.\left.-\left(\frac{mB}{\beta^{2}}\right)^{2}\right]\sin\frac{mB(\delta_{\chi}-z)}{\beta^{2}}+2\lambda_{mBk}\left(\frac{mB}{\beta^{2}}\right)\cos\frac{mB(\delta_{\chi}-z)}{\beta^{2}}\right]\right\}\right\}, \qquad m \geq 1$$

$$N^{s}_{mk}(z) = \frac{1}{\lambda_{mBk}\left[\lambda^{2}_{mBk}+\left(\frac{mB}{\beta^{2}}\right)^{2}\right]}\left\{2\lambda_{mBk}\left(1-\frac{2z}{\delta_{\chi}}\right)-e^{-\lambda_{mBk}z}\left[\lambda_{mBk}\cos\frac{mBz}{\beta^{2}}-\frac{mB}{\beta^{2}}\sin\frac{mBz}{\beta^{2}}\right]\right.$$

$$+e^{-\lambda_{mBk}(\delta_{\chi}-z)}\left[\lambda_{mBk}\cos\frac{mB(\delta_{\chi}-z)}{\beta^{2}}-\frac{mB}{\beta^{2}}\sin\frac{mB(\delta_{\chi}-z)}{\beta^{2}}\right]-\frac{2e^{-\lambda_{mBk}z}}{\delta_{\chi}\left[\lambda^{2}_{mBk}+\left(\frac{mB}{\beta^{2}}\right)^{2}\right]}\left\{\left[\lambda^{2}_{mBk}\right.\right.$$

$$\left.-\left(\frac{mB}{\beta^{2}}\right)^{2}\right]\cos\frac{mBz}{\beta^{2}}-2\lambda_{mBk}\left(\frac{mB}{\beta^{2}}\right)\sin\frac{mBz}{\beta^{2}}\Big]+\frac{2e^{-\lambda_{mBk}(\delta_{\chi}-z)}}{\delta_{\chi}\left[\lambda^{2}_{mBk}+\left(\frac{mB}{\beta^{2}}\right)^{2}\right]}\left\{\left[\lambda^{2}_{mBk}\right.\right.$$

$$\left.\left.\left.-\left(\frac{mB}{\beta^{2}}\right)^{2}\right]\cos\frac{mB(\delta_{\chi}-z)}{\beta^{2}}-2\lambda_{mBk}\left(\frac{mB}{\beta^{2}}\right)\sin\frac{mB(\delta_{\chi}-z)}{\beta^{2}}\right]\right\}\right\}, \qquad m \geq 1$$

TABLE II

VALUES OF $\mathcal{S}^{c}_{mk}$, $\mathcal{S}^{s}_{mk}$, $N^{c}_{mk}$, $N^{s}_{mk}$ FOR SUBSONIC RELATIVE TIP SPEEDS
LIFTING CASE, UNIFORM CHORDWISE LOADING

$$\mathcal{S}^{c}_{mk}(\bar{z}) = e^{-\lambda_{mBk}\bar{z}} \sin\frac{mB\bar{z}}{\beta^2} - e^{-\lambda_{mBk}(\delta_x-\bar{z})} \sin\frac{mB(\delta_x-\bar{z})}{\beta^2} \quad , \quad m \geq 1$$

$$\mathcal{S}^{s}_{mk}(\bar{z}) = e^{-\lambda_{mBk}\bar{z}} \cos\frac{mB\bar{z}}{\beta^2} + e^{-\lambda_{mBk}(\delta_x-\bar{z})} \cos\frac{mB(\delta_x-\bar{z})}{\beta^2} \quad , \quad m \geq 1$$

$$N^{c}_{mk}(\bar{z}) = \frac{1}{\lambda^2_{mBk}+\left(\frac{mB}{\beta^2}\right)^2}\left\{\lambda_{mBk}\left[e^{-\lambda_{mBk}\bar{z}}\cos\frac{mB\bar{z}}{\beta^2} - e^{-\lambda_{mBk}(\delta_x-\bar{z})}\cos\frac{mB(\delta_x-\bar{z})}{\beta^2}\right]\right.$$
$$\left. - \frac{mB}{\beta^2}\left[e^{-\lambda_{mBk}\bar{z}}\sin\frac{mB\bar{z}}{\beta^2} - e^{-\lambda_{mBk}(\delta_x-\bar{z})}\sin\frac{mB(\delta_x-\bar{z})}{\beta^2}\right]\right\} , \; m \geq 1$$

$$N^{s}_{mk}(\bar{z}) = \frac{1}{\lambda^2_{mBk}+\left(\frac{mB}{\beta^2}\right)^2}\left\{\frac{2mB}{\beta^2} - \lambda_{mBk}\left[e^{-\lambda_{mBk}\bar{z}}\sin\frac{mB\bar{z}}{\beta^2} + e^{-\lambda_{mBk}(\delta_x-\bar{z})}\sin\frac{mB(\delta_x-\bar{z})}{\beta^2}\right]\right.$$
$$\left. - \frac{mB}{\beta^2}\left[e^{-\lambda_{mBk}\bar{z}}\cos\frac{mB\bar{z}}{\beta^2} + e^{-\lambda_{mBk}(\delta_x-\bar{z})}\cos\frac{mB(\delta_x-\bar{z})}{\beta^2}\right]\right\} \quad , \quad m \geq 1$$

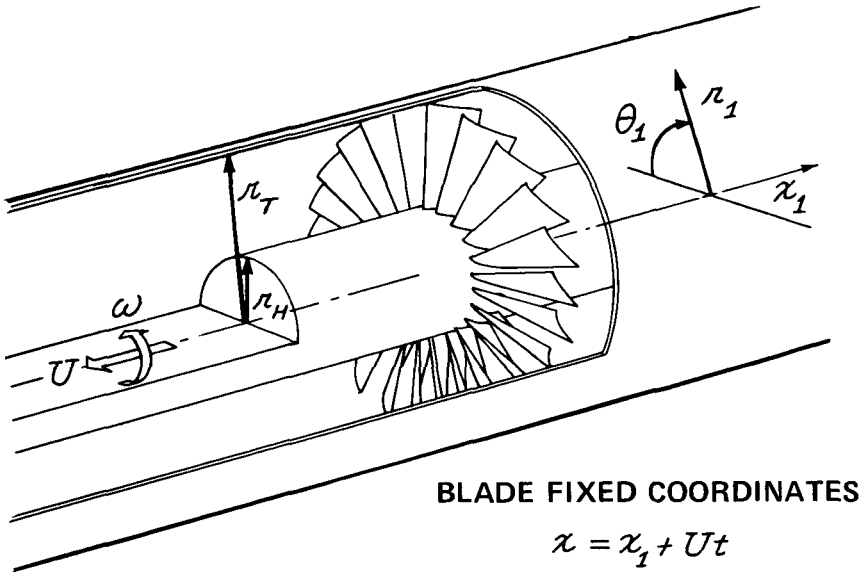


BLADE FIXED COORDINATES

$$x = x_1 + Ut$$

$$\theta = \theta_1 + \omega t$$

$$r = r_1$$

**Figure 1 BLADE GEOMETRY AND FLUID-FIXED COORDINATE SYSTEM**

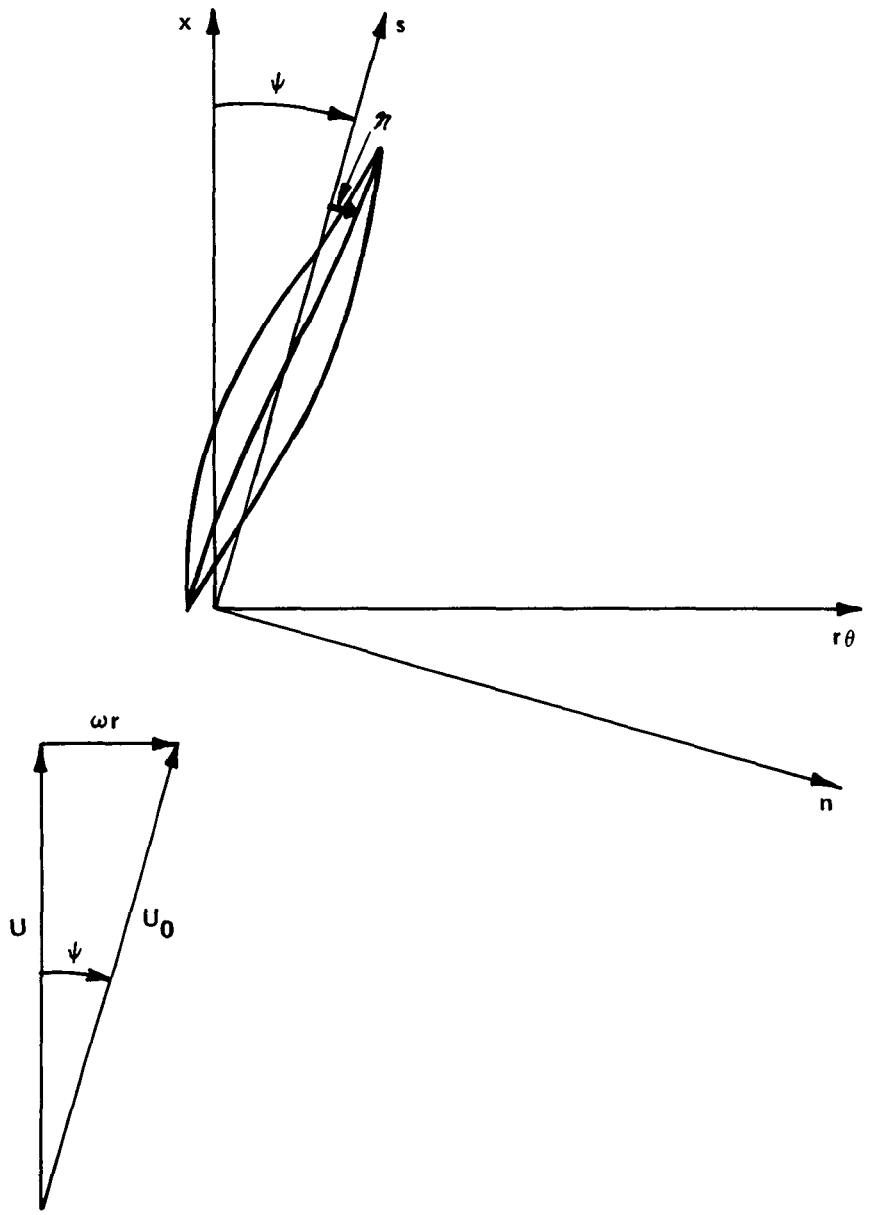


Figure 2 BLADE SECTION AT CONSTANT RADIUS

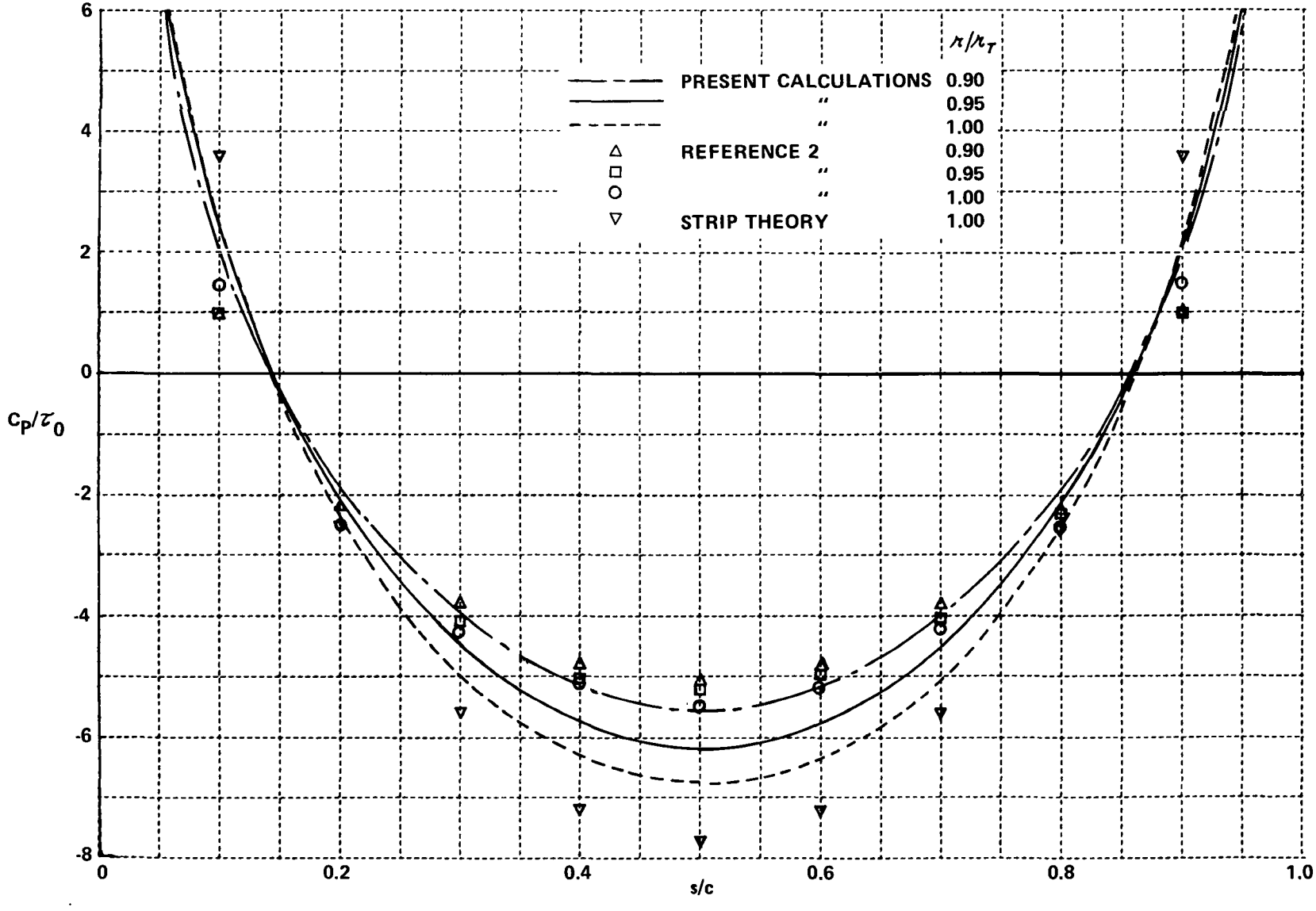


Figure 3 CHORDWISE DISTRIBUTIONS OF PRESSURE COEFFICIENT, NONLIFTING BICONVEX PARABOLIC ARC SECTION, HUB THICKNESS-TO-CHORD RATIO $\tau_o$, B = 64, h = 0.9, $c_a/L_T$ = 0.5, M = 0.6, $M_T$ = 0.775, $M_R$ = 0.98

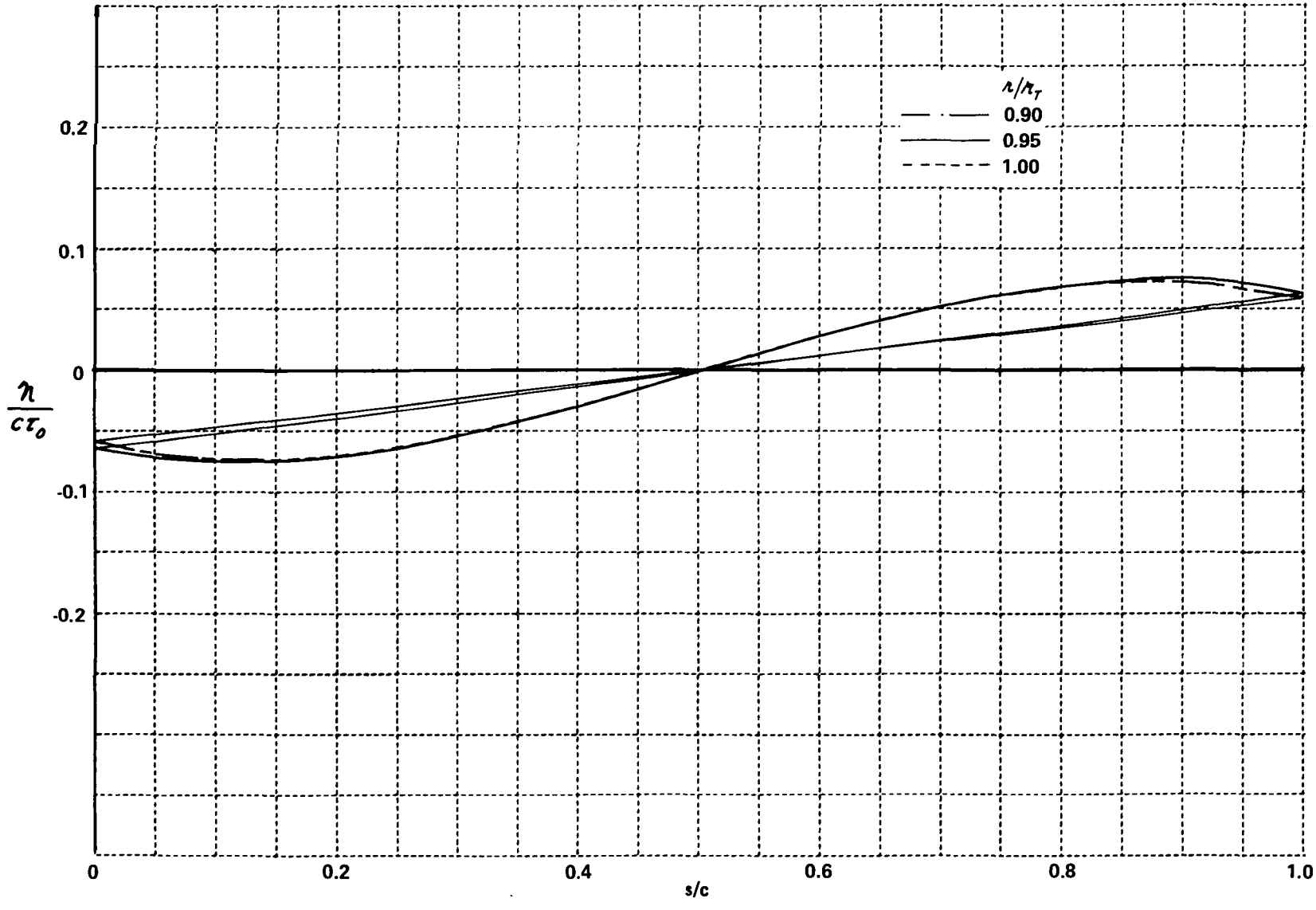


Figure 4 CHORDWISE DISTRIBUTIONS OF BLADE ORDINATES, NONLIFTING BICONVEX PARABOLIC ARC SECTION, HUB THICKNESS-TO-CHORD RATIO $\tau_o$, B = 64, h = 0.9, $c_a/L_T$ = 0.5, M = 0.6, $M_T$ = 0.529, $M_R$ = 0.80

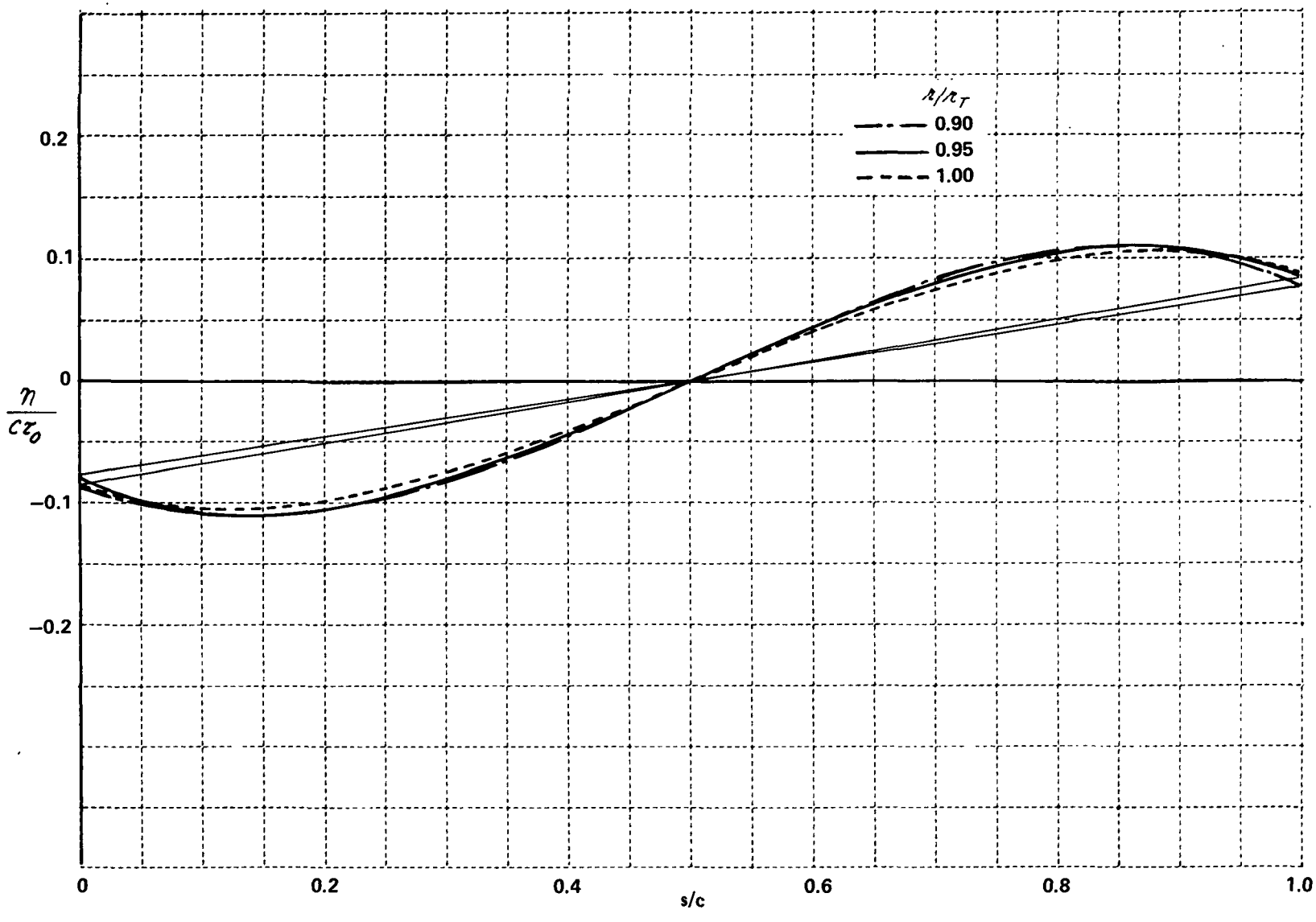


Figure 5 CHORDWISE DISTRIBUTIONS OF BLADE ORDINATES, NONLIFTING BICONVEX PARABOLIC ARC SECTION, HUB THICKNESS-TO-CHORD RATIO $\tau_o$, B = 64, h = 0.9, $c_a/L_T$ = 0.5, M = 0.6, $M_T$ = 0.775, $M_R$ = 0.98

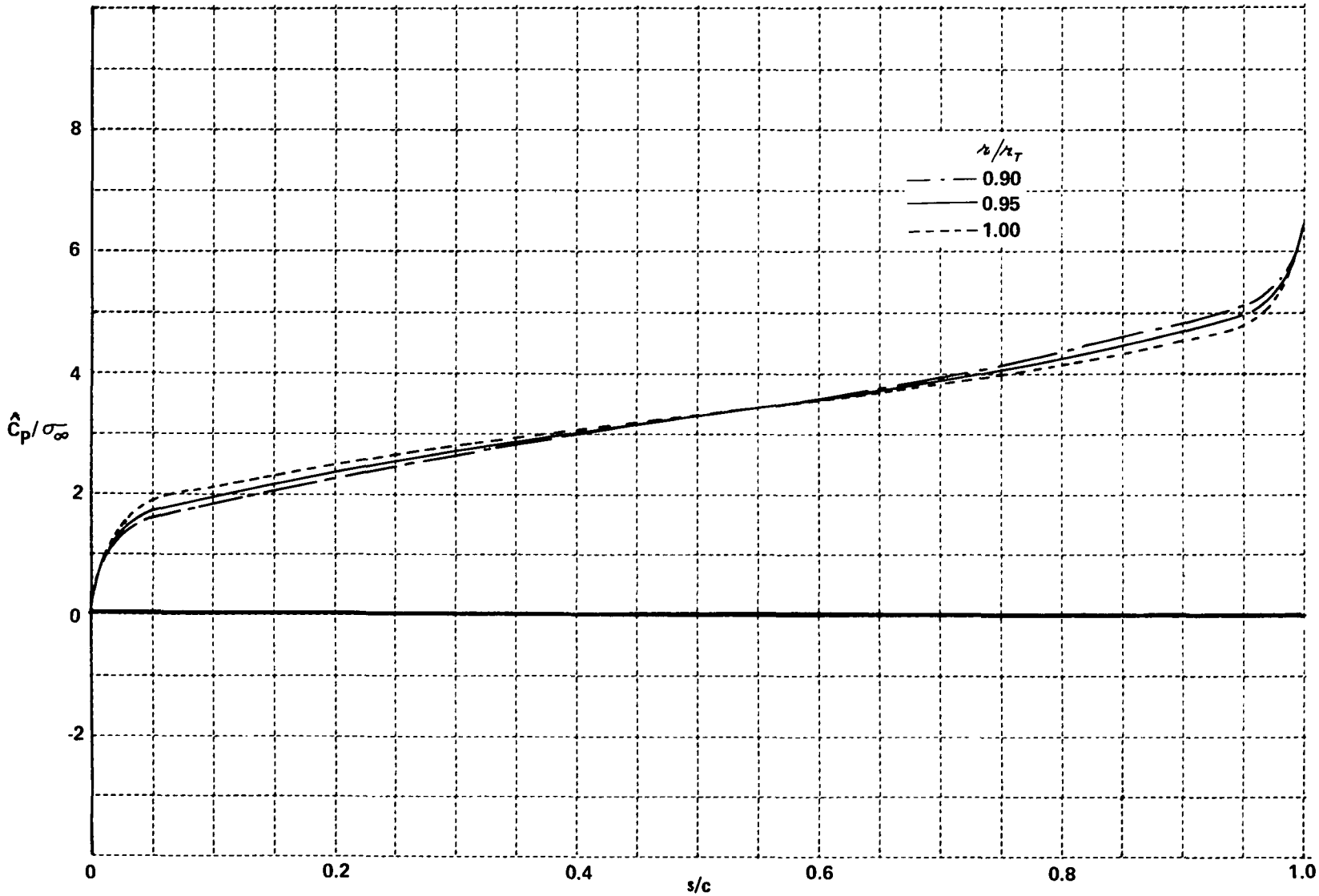


Figure 6 CHORDWISE DISTRIBUTIONS OF PRESSURE COEFFICIENT, UNIFORM CHORDWISE LOADING, CONSTANT WORK DESIGN, NORMALIZED TOTAL PRESSURE RISE $\sigma_\infty$, B = 64, h = 0.9, $c_a/L_T$ = 0.5, M = 0.6, $M_T$ = 0.775, $M_R$ = 0.98

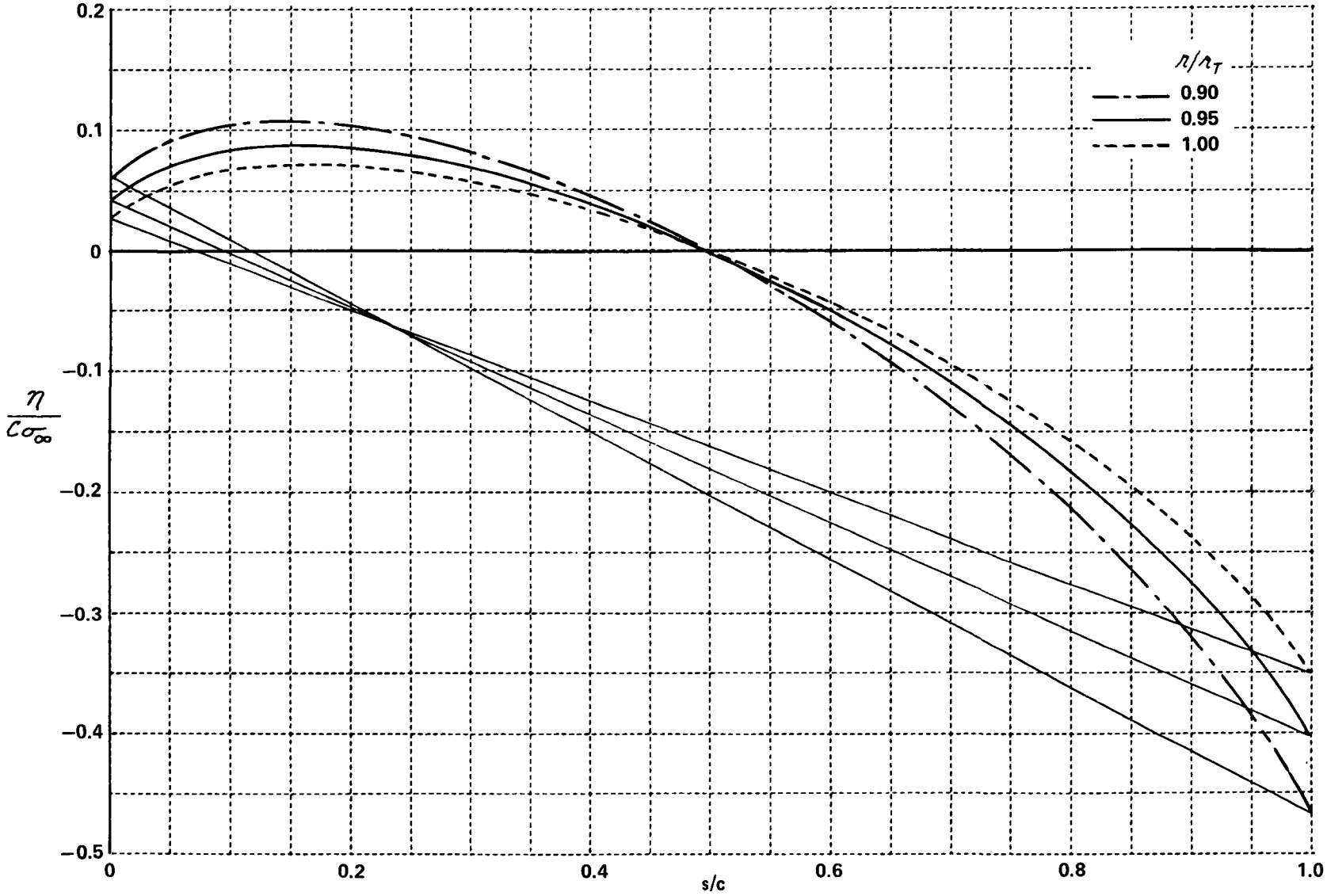


Figure 7 CHORDWISE DISTRIBUTIONS OF BLADE ORDINATES, UNIFORM CHORDWISE LOADING, CONSTANT WORK DESIGN, NORMALIZED TOTAL PRESSURE RISE $\sigma_\infty$, B = 64, h = 0.9, $c_a/L_T$ = 0.5, M = 0.6, $M_T$ = 0.529, $M_R$ = 0.80

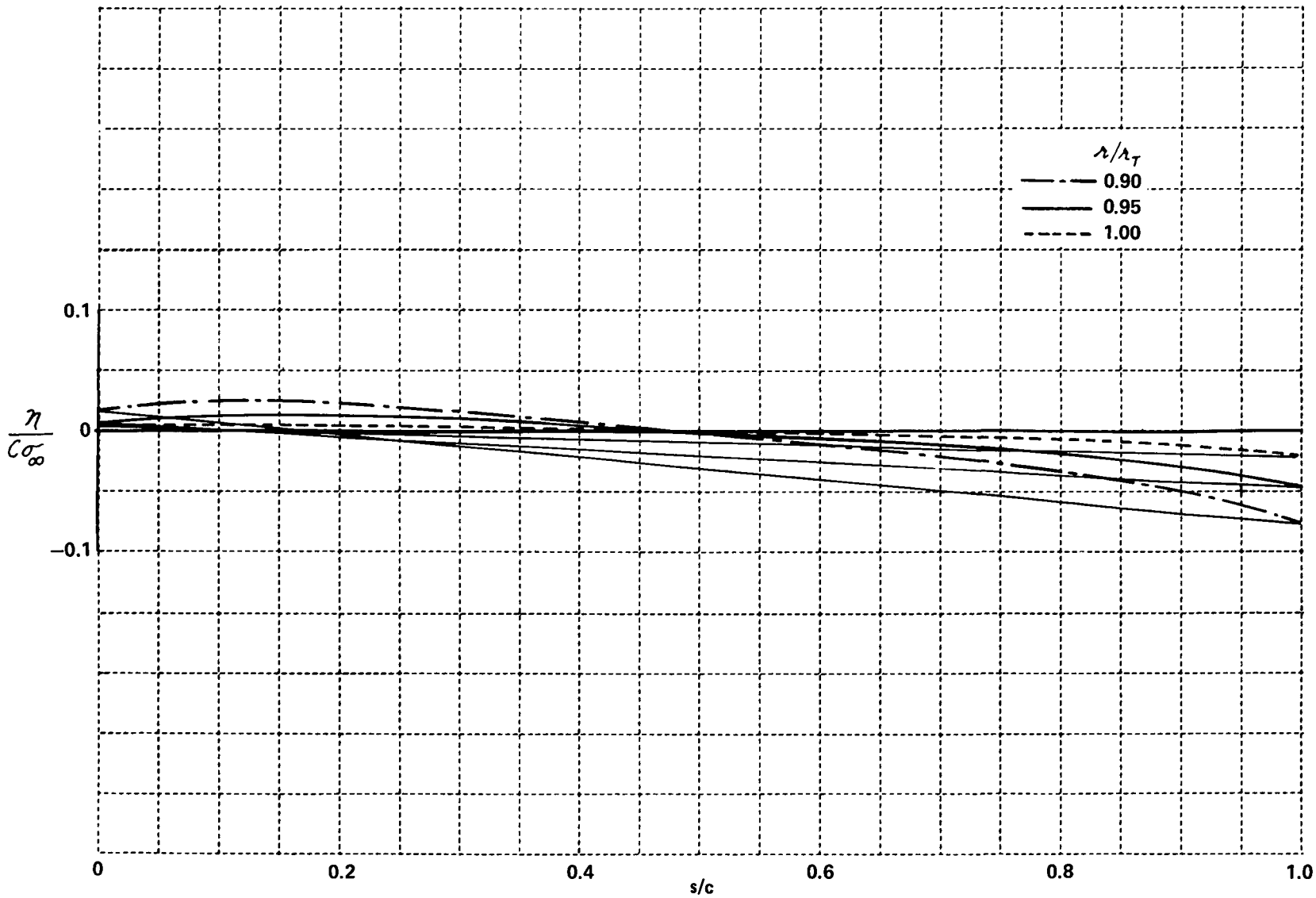


Figure 8 CHORDWISE DISTRIBUTIONS OF BLADE ORDINATES, UNIFORM CHORDWISE LOADING, CONSTANT WORK DESIGN, NORMALIZED TOTAL PRESSURE RISE $\sigma_\infty$, B = 64, h = 0.9, $c_a/L_T$ = 0.5, M = 0.6, $M_T$ = 0.775, $M_R$ = 0.98